ACADEMIC
PRESS

One-eyed pinhead regulates cell motility independent of Squint/Cyclops signaling

Rachel M. Warga* and Donald A. Kane

Department of Biology, University of Rochester, Rochester, NY 14627, USA

Abstract

In vertebrates, EGF-CFC factors are essential for Nodal signaling. Here, we show that the zygotic function of *one-eyed pinhead,* the zebrafish EGF-CFC factor, is necessary for cell movement throughout the blastoderm of the early embryo. During the blastula and gastrula stages, mutant cells are more cohesive and migrate slower than wild-type cells. Chimeric analysis reveals that these early motility defects are cell-autonomous; later, *one-eyed pinhead* mutant cells have a cell-autonomous tendency to acquire ectodermal rather than mesendodermal fates. Moreover, wild-type cells transplanted into the axial region of mutant hosts tend to form isolated aggregates of notochord tissue adjacent to the mutant notochord. Upon misexpressing the Nodal-like ligand Activin in whole embryos, which rescues aspects of the mutant phenotype, cell behavior retains the *one-eyed pinhead* motility phenotype. However, in *squint;cyclops* double mutants, which lack Nodal function and possess a more severe phenotype than zygotic *one-eyed pinhead* mutants, cells of the dorsal margin exhibit a marked tendency to widely disperse rather than cohere together. Elsewhere in the double mutants, for cells of the blastoderm and for rare cells of the gastrula that involute into the hypoblast, motility appears wild-type. Notably, cells at the animal pole, which are not under direct regulation by the Nodal pathway, behave normal in *squint;cyclops* mutants but exhibit defective motility in *one-eyed pinhead* mutants. We conclude that, in addition to a role in Nodal signaling, One-eyed pinhead is required for aspects of cell movement, possibly by regulating cell adhesion.
© 2003 Elsevier Inc. All rights reserved.

Keywords: Epiboly; Involution; Convergence; Cell adhesion; Motility; *one-eyed pinhead*; Nodal

Introduction

Members of the EGF-CFC gene family, such as mouse and human *cripto, Xenopus FRL-1* and zebrafish *one-eyed pinhead (oep),* encode extracellular molecules essential during early vertebrate development (Schier and Shen, 2000). These genes also may play a role in oncogenesis. The first member of this family, *cripto,* was identified as a gene expressed in undifferentiated human teratocarcinoma cells (Salomon et al., 1999), and it has since been found to be expressed at elevated levels in a wide variety of metastatic tissues (Salomon et al., 2000). While much is known about the biochemical nature of these molecules and the signaling pathways in which they participate, less is known about the cellular processes that EGF-CFC molecules control.

EGF-CFC proteins are characterized by a region with homology to Epidermal Growth Factor (EGF) and a unique conserved cysteine-rich region known as the CFC domain. Additionally, the proteins contain a signal sequence and a C-terminal hydrophobic domain (Shen et al., 1997). Mouse Cripto has further been demonstrated to be anchored to the plasma membrane by a glycosylphosphtidylinositol (GPI) moiety (Minchiotti et al., 2000), and all EGF-CFC members except FRL-1 contain potential GPI modification sites in their C terminus (Shen et al., 1997). Hence, the sequence data indicate that the protein acts at the cell membrane, and cell autonomy experiments in zebrafish support the idea that these molecules lie at the cell surface and participate in near neighbor interactions (Gritsman et al., 1999; Schier et al., 1997; Strähle et al., 1997).

The developmental role of these molecules has been elucidated by the study of mutations in mouse and zebrafish. In mouse, knockout of gene function demonstrated that

* Corresponding author. Fax: +1-585-275-2070.

E-mail address: rachel_warga@urmc.rochester.edu (R.M. Warga).

cripto is necessary for normal formation of the anterior–posterior axis during gastrulation (Ding et al., 1998; Xu et al., 1999), a process thought to be regulated by complimentary cell movements in the visceral endoderm and epiblast (Tam et al., 2001). Additionally, most of the embryonic mesendoderm is abrogated in the mutant (Ding et al., 1998; Xu et al., 1999). In zebrafish, the Cripto ortholog was identified by mutation and subsequent cloning of the locus *one-eyed pinhead* (Hammerschmidt et al., 1996; Schier et al., 1996; Solnica-Krezel et al., 1996; Strähle et al., 1997; Zhang et al., 1998). The phenotype of the zebrafish mutant possesses some similarities to the mouse mutant. However, because the *oep* transcript is present both maternally and zygotically, only by breeding adult rescued homozygous *oep* mutants can one produce an extreme phenotype, termed a maternal-zygotic phenotype, that more closely resembles *cripto* mutant embryos (Gritsman et al., 1999).

Zebrafish embryos lacking zygotic *oep* function fail to form adequate amounts of mesendoderm and later display neural defects and cyclopia. Embryos lacking both maternal and zygotic *oep* function form almost no mesendoderm and have an altered anterior–posterior axis. Both mesendoderm formation and elongation of the axis are driven by stereotypic cell movements occurring in the zebrafish gastrula (Warga and Kimmel, 1990), and inspection of maternal-zygotic *oep* mutants has shown that these movements are abnormal (Carmany-Rampey and Schier, 2001; Gritsman et al., 1999). Interestingly, the appearance of maternal-zygotic *oep* embryos closely resembles embryos doubly mutant for the *nodal*-related genes *squint* and *cyclops* (Feldman et al., 1998). This similarity and subsequent studies have led to the hypothesis that EGF-CFC molecules are required for the action of Nodal ligands (Schier and Shen, 2000; Whitman, 2001), important growth factors involved in early embryonic decisions. Biochemical analyses of Cripto support this idea. The interaction of Cripto with Alk4 is necessary for Nodal ligand binding to the Alk4/ActR-IIB receptor complex and for Smad2 activation by Nodal (Reissmann et al., 2001; Yan et al., 2002; Yeo and Whitman, 2001). Activin, a related TGF-β molecule with similar inducing properties as Nodal ligands (Massagué, 1998; Schier and Shen, 2000), activates Smad2 independently of Cripto function. Hence, misexpression of Activin in zebrafish embryos—but not the combination of both Nodal ligands Squint and Cyclops together—rescues aspects of the *oep* mutant phenotype that are the result of defective Squint/Cyclops signaling (Gritsman et al., 1999).

Other signaling pathways may also require the participation of EGF-CFC molecules. For example, studies of differentiated cells have led to the hypothesis that EGF-CFC molecules participate in mitogen-activated protein kinase (MAPK) signaling, a pathway which has a well known role in controlling cell adhesiveness, cell shape, and cell migration (Hagemann and Blank, 2001; Kassis et al., 2001). Biochemical analysis indicates that Cripto indirectly activates the erb B-4 receptor (Bianco et al., 1999) and enhances activation of the cytoplasmic tyrosine kinase Shc, leading to the subsequent downstream activation of MAPK (Kannan et al., 1997). Analogous to that seen in metastasizing tumors, Cripto misexpressing epithelial cells undergo an epithelial–mesenchymal transition and show increased motility (Weschselberger et al., 2001), behaviors which are blocked by specific MAPK inhibitors. Because Nodal and Alk4 are not required for Cripto stimulation of the *ras/raf/MEK/MAPK* signaling cascade, it seems likely that both pathways act independent of one another (Bianco et al., 2002).

Here, we characterize the phenotype of motile cells in zygotic mutants of *oep*. We show the requirement of *oep* function, beginning early in the blastula, for characteristic cell movements of the zebrafish mesendoderm and document that alteration in cell movement occurs before changes in cell fate as assayed by the transcription of genes downstream of the zebrafish Nodal signaling pathway. Notably, we find that mutant cells are abnormally cohesive and move slower than wild-type cells. In accord with previous studies on autonomy of Oep function, these defects in cell behavior are cell-autonomous. While injecting Activin rescues many aspects of the mutant phenotype, it does not rescue defects in cell movement or cohesiveness. We also find no evidence for a similar motility defect in the *squint;cyclops* double mutant. Moreover, cells of the animal pole in *oep* mutant blastula transiently display similar defects in motility similar to that observed at the margin even though the animal pole is thought to be devoid of Squint and Cyclops signaling (Thisse et al., 2000). We conclude that one significant function of zebrafish Oep is to delicately balance interactions between neighboring cells during early morphogenesis, and that this function is independent of a cellular response to the zebrafish Nodal-related signaling molecules Squint and Cyclops.

Materials and methods

Cell labeling and time-lapse analysis

Embryos were derived from crosses of identified *oep* heterozygotes of two ENU generated alleles, oep^{tz257} and oep^{m134}, which were used interchangeably in all experiments and were found to give identical phenotypes at both the cytological and morphological level. Embryos were also derived from crosses of fish that were doubly heterozygous for the $cyclops^{m294}$ and $squint^{cz35}$ alleles.

Between the 1000- to 2000-cell stage, a single cell was labeled with 5% rhodamine–dextran or additionally 2% biotinylated dextran (a fixable tracer), as described by Warga and Nüsslein-Volhard (1999). Between 6 and 12 embryos were mounted between cover glasses sealed with Vaseline in 0.1% agarose and 100× Danieau's media. Recordings were made on a Zeiss Axiophot II equipped with the Märzhauser x-y stage controlled by the Multicontrol-

2000 controller which allowed for the simultaneous recording of many embryos using a low-light intensified camera (ICCD-350F, Videoscope). Multiplane imaging and data storage were as described by Kane et al. (1996). Data were stored directly onto a Power Macintosh 9600/350 running Cytos 3.0.1 software (Applied Scientific Instrumentation). Figures were produced with Adobe Photoshop 6.0.

Data analysis

Cell volume was calculated by importing an image of the cell into NIH video and running a macro program that measured the number of pixels inside of the cell outline, the long axis (length) and short axis (width), both in pixels. Depth (z) was measured by using the output from the motorized stage on a Zeiss Axiophot II onto a Power Macintosh 9600/350 running Cytos 3.0.1 software. All ad hoc pixel units of measure were then converted to metric units.

For measurement of cell scatter during early epiboly, we compared clones of equivalent cell number in wild-type and mutant siblings at 40% epiboly. The point-to-point distance from the center of one cell to the center of all other cells in the clone was measured and then repeated for each cell of the clone. Hence, disregarding duplicated measurements, a clone of four cells would have six individual measurements, as shown in the example in Fig. 3C.

For measurement of dorsal and vegetal displacement during early epiboly, the point-to-point distance that a cell moved dorsovegetally between the sphere to 40% epiboly stage was measured compared to clonally related extraembryonic surface cells as a fixed reference (see Fig. 3D).

Rate and line tracings of cell movement were calculated from time-lapse video segments imported into NIH video and analyzed using a macro that stored x, y, z (plane), and t (time) for designated cells from frame to frame. Extraembryonic surface cells were used to fix the x-reference point; the y-axis was not controlled. The output for this file was read by a second macro which converted the data into a line tracing of cell movement correcting for x, y, and z drift (experimentally caused by refocusing and repositioning or naturally caused due to epiboly and rotation of the embryo). Alternatively, the file was brought into a spread sheet program, which was used to calculate rates of movement.

Cell transplantation

Transplantation was carried out between doming and 30% epiboly stage as described by Ho and Kane (1990). Hosts were examined at shield stage and again at 24 h, after which hosts were examined daily until cells of the transplant were fully differentiated.

Immunohistochemistry and RNA in situ hybridization

Embryos injected with biotinylated-dextran were processed as described in the zebrafish book (Westerfield, 1993).

Antibody staining was carried out as described by Warga and Nüsslein-Volhard (1999). RNA in situ hybridization was carried out as described by Thisse and Thisse (1994).

Mutant genotype was both determined by sorting for the live phenotype during epiboly or genotyping afterwards as described below. Both methods gave equivalent results.

Genotyping

In experiments requiring genotyping of *oep* mutant embryos, we created *trans*-heterozygotes between both the oep^{tz257} allele and the oep^{m134} allele and identified the progeny as follows: Using the *oep* sequence (Zhang et al., 1998), we created the following primers: tz257 (F: 5′-CGAGTG-GAGATGTTCTAATGGTG-3′) and (R: 5′-CGAACAGTT-GACTCGTCAC-3′); m134 (F: 5′-GCTCCCTCAGAA-CACTGTA-3′) and (R: 5′-GAGAGCTGCTTCCTTCTC-3′), which took advantage of the single base pair substitution in each *oep* allele and which specifically amplified by PCR the mutant allele and not the wild-type allele at high stringency (62°C annealing). Each embryo was scored for the presence or absence of the product on an agarose gel. As *oep* is a recessive mutation, both alleles must be mutant for the phenotype to be visible, and thus two products must be amplified.

In this study, we could see no phenotypic difference between the homozygous mutants, oep^{tz257}/oep^{tz257} and oep^{m134}/oep^{m134}, and we could see no differences between the *trans*-heterozygous mutant oep^{tz257}/oep^{m134} and either of the homozygous mutants.

In experiments using *squint;cyclops* mutant embryos, genotype was determined by PCR. For *squint,* we used primers which identified the presence or absence of the 1.9-kb insertion into the $squint^{cz35}$ mutant allele of *znr2* (Feldman et al., 1998). For *cyclops,* we used primers which amplified the Cys to Arg conversion in the $cyclops^{m294}$ mutant allele of *znrl* detected by *Age*I digest (Sampath et al., 1998).

mRNA misexpression

Xactivinβ-B (Sokol et al., 1991) was linearized with *Eco*RI, and zf-heat shock-Green Fluorescent Protein (gift of Dave Raible) was linearized with *Not*I. Sense strand-capped mRNA was synthesized by using the SP6 mMESSAGE mMACHINE system (Ambion). *Xactivinβ-B* mRNA was diluted in distilled water and microinjected into the blastoderm at the one-cell stage at a final concentration of ~0.25 pg. Uninjected siblings or control embryos injected with *Green Fluorescent Protein* mRNA (~10 pg) did not exhibit a rescued phenotype or perturbations in cell movement.

Results

This work focuses on aspects of general cell motility that are defective in the *oep* mutant, a phenotype which we term

"*oep* mediated cell motility." In order to separate specific functions of *oep* on cell motility from the more general functions of the zebrafish Nodal pathway on cell specification, we examined the zygotic rather than the maternal-zygotic *oep* mutant. The zygotic pattern of *oep* transcripts comes up between 4 and 5 hours postfertilization, initially overlapping with the maternal pattern of *oep* transcripts. At this time, both transcripts are uniformly expressed throughout the zebrafish blastoderm. However, by 5–6 h, before the onset of gastrulation, expression becomes restricted to the margin of the blastoderm and the maternal transcript is no longer detectable as assayed in zygotic *oep* deletions (Zhang et al., 1998). Although the rate of decay of residual protein is unknown, we show that the *oep*-dependent cell motility phenotype in the 4-h mutant, i.e., an hour after the transcriptional activation at Mid-Blastula Transition (Kane and Kimmel, 1993), is indistinguishable from that seen later, arguing that the activity of the *oep* protein must correlate roughly with the concentration of the observed *oep* transcript. In contrast, we demonstrate that the maternally contributed *oep* activity is sufficient for initiation of major specification events in the blastula that require the Nodal pathway. Thus, zygotic *oep* mutants display an interesting phenotype, one where Oep activity is initially functional but later absent or almost absent. Therefore, analysis of the zygotic *oep* mutants should reveal cellular defects that are independent of the general downstream effects of the zebrafish Nodal signals, Squint and Cyclops.

Morphologically abnormal cells in the hypoblast of oep mutants

To elucidate the role of *oep* in morphogenesis, we labeled individual precursor cells of the mesendoderm with lineage tracer in wild-type and *oep* mutant blastulae and examined the morphology of the clonal progeny in the late gastrulae. In normal embryos, the mesendodermal germ layer, known as the hypoblast, originates from involuting cells at the margin of the blastoderm (Warga and Kimmel, 1990). The first involuting cells appear large and flat, have extensive filopodia, and actively separate from one another (Fig. 1A and C), presumably using the yolk cell membrane as a substrate (Warga and Nüsslein-Volhard, 1999). In mutant embryos, the first involuting cells were atypically small and spherical and had stumpy filopodia (Fig. 1B and D). Based on height and area measurements, these cells had normal cell volumes (Fig. 1E). A most unusual feature of mutant hypoblast cells was their tendency to adhere to one another, particularly clonal relatives. Moreover, they were attached poorly to their normal substrate, the yolk cell (Fig. 1F and G). Both mutant alleles of *oep* exhibited these changes in cell morphology and cohesivity to the same degree.

Recording of live mutant embryos, with time-lapse video microscopy using DIC bright field optics revealed that presumptive mesendoderm cells in the *oep* embryo began to compact together shortly before the onset of involution. As gastrulation begins, these marginal cells normally disaggregate and begin involuting (Fig. 2A) to form the hypoblast layer. In mutant blastulae, the marginal cells appeared more attached to one another, and this coupled-like morphology persisted as cells began involuting (Fig. 2A'). After involuting, hypoblast cells in wild-type embryos become mesenchymal, whereas hypoblast cells in mutant embryos became increasingly more attached to one another (Fig. 2B and C). This abnormal behavior occurred both dorsally and laterally, and persisted throughout gastrulation. By mid gastrulation, cells of the axial hypoblast became hyperaggregated and cells of the paraxial mesoderm and endoderm were unusually clumped (Fig. 2D and E), resembling the cells fixed and stained in Fig. 1. In summary, marginal cells in the *oep* mutant behave abnormally before and after cells enter the hypoblast, and this change in behavior correlates with the observed changes in morphology.

Cell movement is altered in oep mutants

To examine cellular movement of individual cells, we labeled single blastomeres at the 2000-cell stage with rhodamine–dextran and, beginning immediately afterward, examined cellular rearrangements by time-lapse video. This technique reveals the behavior of single cells and their ensuring progeny as they separate from each other and disperse into the surrounding unlabeled neighbors. Normally, the progeny of a single marginal cell labeled at the 2000-cell stage tend to scatter during the morphogenesis that occurs during early epiboly (Fig. 3A). This scattering movement begins subtly with the establishment of cell motility that begins at the Mid-Blastula Transition, and then the movement becomes more apparent at dome stage, when the radial intercalation of deeper cells amongst more superficial cells thins and spreads the blastoderm over the yolk cell in epiboly (Helde et al., 1994; Kane and Kimmel, 1993; Warga and Kimmel, 1990). Shortly following the onset of epiboly, labeled cells are also drawn dorsally and vegetally by dorsal compaction, a subtle movement which is mediated by increased cell cohesiveness in the organizer region (Warga and Nüsslein-Volhard, 1998, 1999). At the beginning of gastrulation, labeled cells begin to move to the edge of the blastoderm and involute singly deep into the embryo where they reverse their direction and migrate towards the animal pole. Afterwards, these cells migrate dorsally and spread apart along the animal–vegetal axis in a movement known as convergent-extension, a cell rearrangement mediated by mediolateral cell intercalations (Schmitz and Campos-Ortega, 1994; Warga and Kimmel, 1990).

The underlying cell behaviors of each of these cell movements were impaired in *oep* mutant blastulae (Fig. 3A'). During early epiboly, rather than scatter, clones of labeled marginal cells remained in close contact with sibling cells (Fig. 3B). These differences were all statistically significant (Fig. 3C), even dorsally, where the magnitude of the cell scatter is already reduced. During dorsal compaction, mutant cells failed to move dorsally and vegetally (Fig. 3D; Table 1). During gastrulation, mutant cells involuted, but
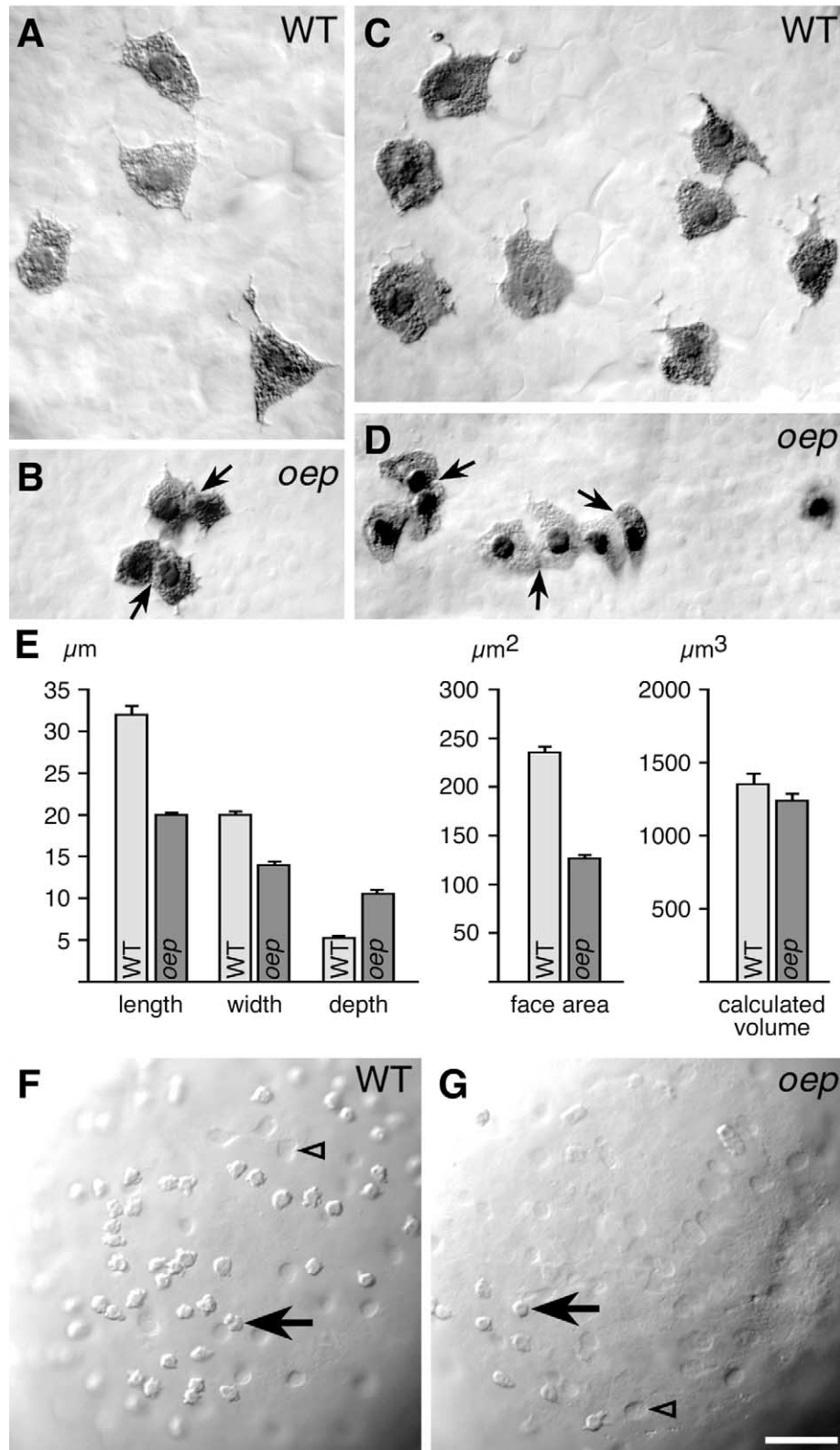
Fig. 1. Hypoblast cells in the *oep* mutant have abnormal morphology and display abnormal cell–cell interactions. (A–D) Hypoblast cells from clones labeled with biotinylated-dextran at the 2000-cell stage. Embryos were fixed at 90% epiboly and stained for biotinylated-dextran. (A, B) Two divisions postinjection. (C, D) Three divisions postinjection. Mutant hypoblast cells are tightly coupled to one another (arrows). During these analyses, no obvious differences in cell division were detected. (E) The average length (long axis), width (short axis), depth (z-axis), face area (length × width), and calculated volume (face area × depth) of biotin-labeled hypoblast cells (96 cells in 14 wild-type embryos; 46 cells in 6 mutant embryos). The yolk cell surface of (F) wild-type and (G) mutant sibling, after surgical removal of the blastoderm at 80% epiboly. Cells (big arrow) remaining attached to the mutant yolk cell (5 ± 1 cells; $n = 15$ embryos) were significantly fewer than on the yolk cell of wild-type siblings (272 ± 15 cells; $n = 15$ embryos) compared using the Wilcoxon Rank Sum Test ($P < 0.0001$). Arrowheads indicate yolk cell nuclei. Scale bar: 10 μm (A–D), 40 μm (F–G).
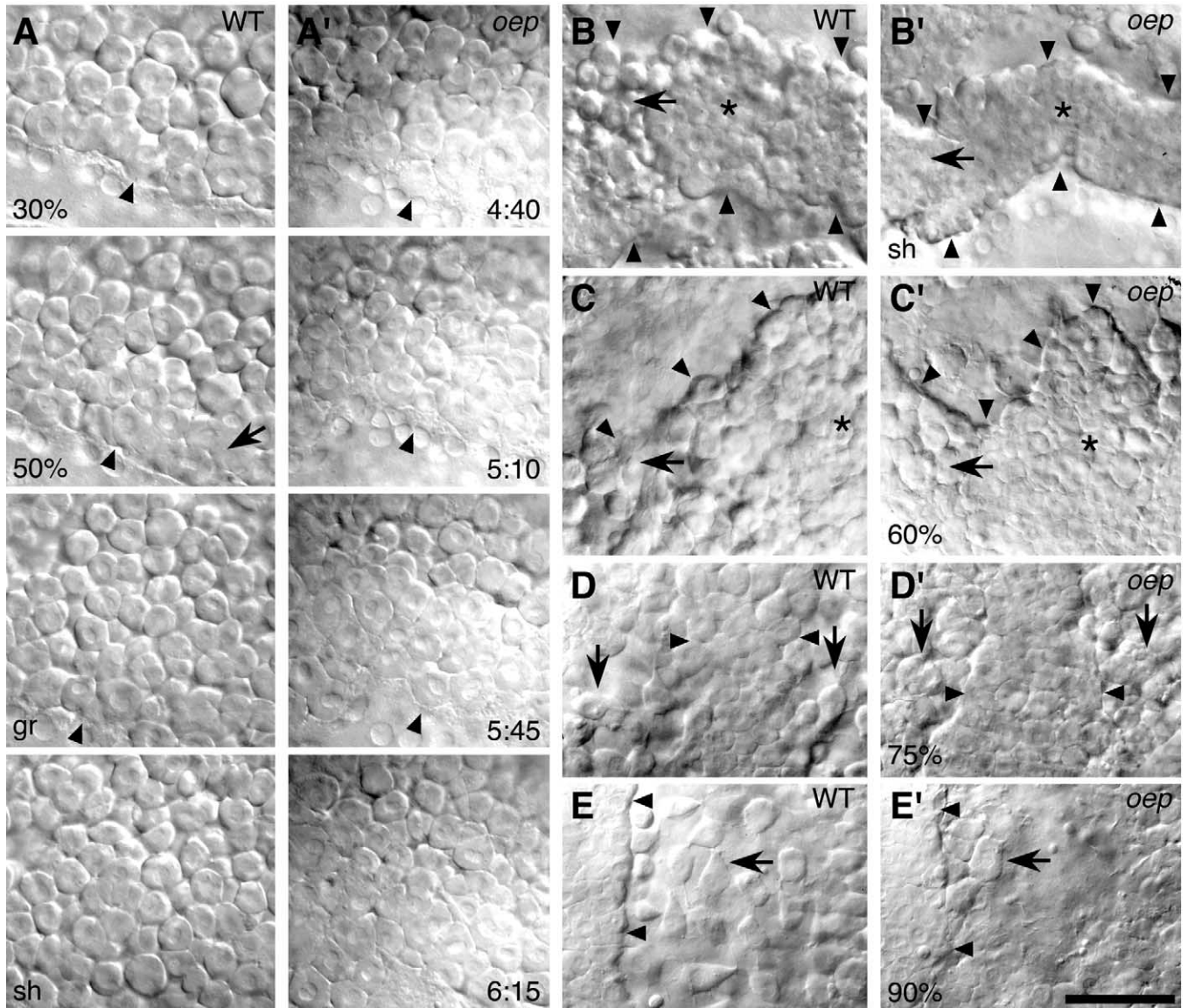
Fig. 2. The *oep* mutation affects morphogenesis of the hypoblast. (A) Selected frames from time-lapse recordings of the lateral side of wild-type and mutant siblings during early epiboly. Views are near the surface of the blastoderm, just beneath the enveloping layer. The margin of the blastoderm (arrowheads) is to the lower edge of the field. Cells in the wild-type appear rounded and loosely aggregated, except at the edge of the margin at 50% epiboly when cells coalesce together before preparing to involute (black arrow). Cells in the mutant appear more coherent than in wild-type, and due to increased cell contact become optically more refractive; time after fertilization: h:mm. (B–E) The forming hypoblast layer of wild-type and mutant siblings. Views are in the deepest layers of the blastoderm. (B, C) During early gastrulation, dorsal hypoblast cells in wild-type embryos disaggregate and begin to acquire a mesenchymal appearance (arrows), except at the midline (asterisk) where cells tend to condense together. Dorsal hypoblast cells in mutant embryos do not dissociate, but rather become more tightly coupled (arrows); arrowheads outline the hypoblast. (B) Shield stage. (C) 60% epiboly, note the jagged edge to the mutant hypoblast instead of the normal taper from the midline. (D, E) By mid- and late gastrulation, axial hypoblast cells in wild-type embryos have consolidated into a morphological structure (arrowheads), whereas the paraxial hypoblast cells (black arrows) form isolated individual mesenchymal cells. Axial hypoblast cells in mutant embryos are hyperaggregated (arrowheads) and the paraxial hypoblast cells are atypically clumped (arrows). (D) 75% epiboly. (E) 90% epiboly. Scale bar: 30 μm.

seldom as individuals, and always slower in comparison to cells in wild-type siblings (Fig. 3A′). Finally, during convergent extension, rather than extending apart along the anterior–posterior axis, mutant cells remained cohered and did not extend. Also, these cells converged more slowly toward dorsal (Fig. 3E). In sum, *oep* mutant cells appeared to be generally crippled in their ability to move during the normal cellular rearrangements that drive morphogenesis. However, despite these conspicuous defects in cell motility,

labeled mutant cells eventually integrate into the forming embryo, and later differentiate into the appropriate endodermal and/or mesodermal derivatives (data not shown).

Defective cell motility is autonomous to oep mutant cells

To test whether defective cell motility is intrinsic to individual cells in *oep* mutants, groups of cells from mutant and wild-type donors were mixed together and transplanted
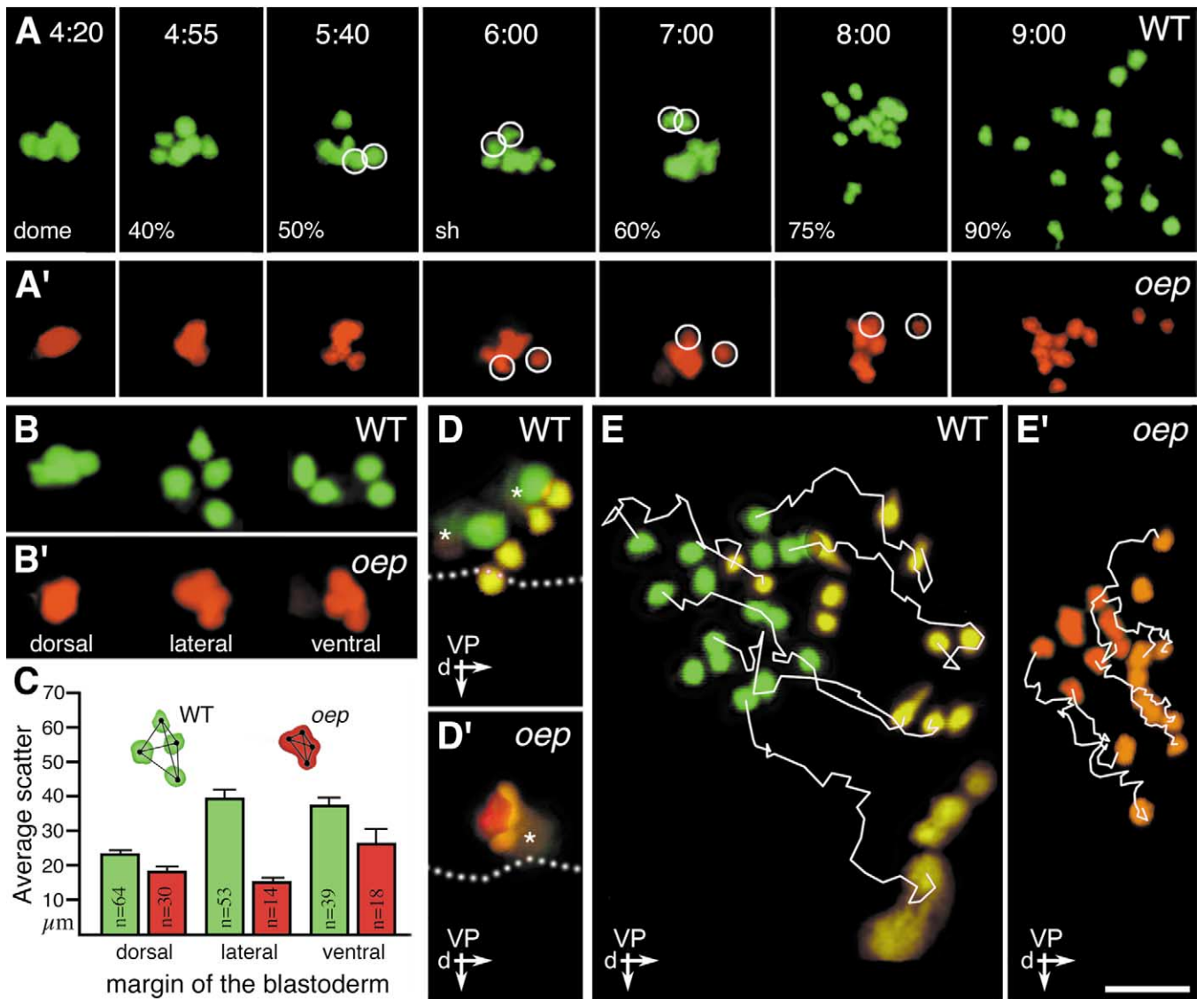
Fig. 3. Movement of the marginal cells is impaired in *oep* mutants. (A) Clones of cells in sibling embryos at the ventral margin. At the onset of the recording each clone was four cells. Between doming and 40% epiboly, the wild-type clone scatters. By 50% epiboly, dorsal compaction has also drawn the wild-type clone more dorsally (the slight displacement right), which is not so apparent in a ventral clone. Between 50% epiboly and 60% epiboly, cells in the wild-type clone involute; circles indicate the first cells which will involute at 50% epiboly, and have already done so by shield stage as they migrate away from the margin deep in the hypoblast layer. Between 75 and 90% epiboly, the wild-type clone extends apart because of the cell rearrangements of convergent-extension. By contrast, cells in the mutant clone remain coupled to one another throughout all of these movements, neither scattering nor moving dorsally between doming and 40% epiboly and involuting and converging more slowly during gastrulation. (B) Clonal scatter by radial intercalation at dorsal, lateral, and ventral locations in six individuals at 40% epiboly stage. Each clone is equal in number, four cells. The wild-type clones are scattered except for the dorsal clone that has already consolidated due to dorsal compaction, the mutant clones regardless of location are consolidated. (C) The median distance between clonal cells at 40% epiboly depending on dorsoventral location. Distance was calculated as the center to center distances between each combination of cells, as described in Materials and methods. Mutant clones significantly differ from wild-type controls at $P < 0.001$ for Wilcoxon Rank Sum Test. (D) Dorsovegetal movement by dorsal compaction. Between sphere (green) and 40% epiboly (yellow), two cells in a wild-type clone divide and move dorsovegetally. Between sphere (red) and 40% epiboly (orange), the two cells in a mutant divide but do not move. Asterisk indicates clonally related extraembryonic surface cells used for reference; dotted line indicates blastoderm margin; arrows indicate orientation: dorsal (d), vegetal pole (VP). (E) Convergent-extension movement. Between 70% (green) and 90% epiboly (yellow), cells in a wild-type clone converge rapidly toward dorsal while extending apart along the animal–vegetal axis. Between 70% (red) and 90% epiboly (orange), the cells in a mutant clone converge more slowly and extension along the animal–vegetal axis is extremely reduced. The tracings follow selected cells from each clone at 3-min intervals. Wild-type rate of movement was significantly faster during gastrulation (220 ± 10 μm/h; $n = 16$ cells in 3 embryos) than mutant (90 ± 8 μm/h; $n = 16$ cells in 3 embryos) ($P < 0.0001$) compared using the Wilcoxon Rank Sum Test. Scale bar: 100 μm (A), 50 μm (B, D, E).

into the mesendodermal progenitor field of host blastulae. Within an hour after transplantation, mutant and wild-type donor cells began to separate from one another, indicating a difference in the ability for these cells to migrate (Fig. 4A–C). Typically, the mutant cells advanced more slowly toward the dorsal side of the embryo during the period of
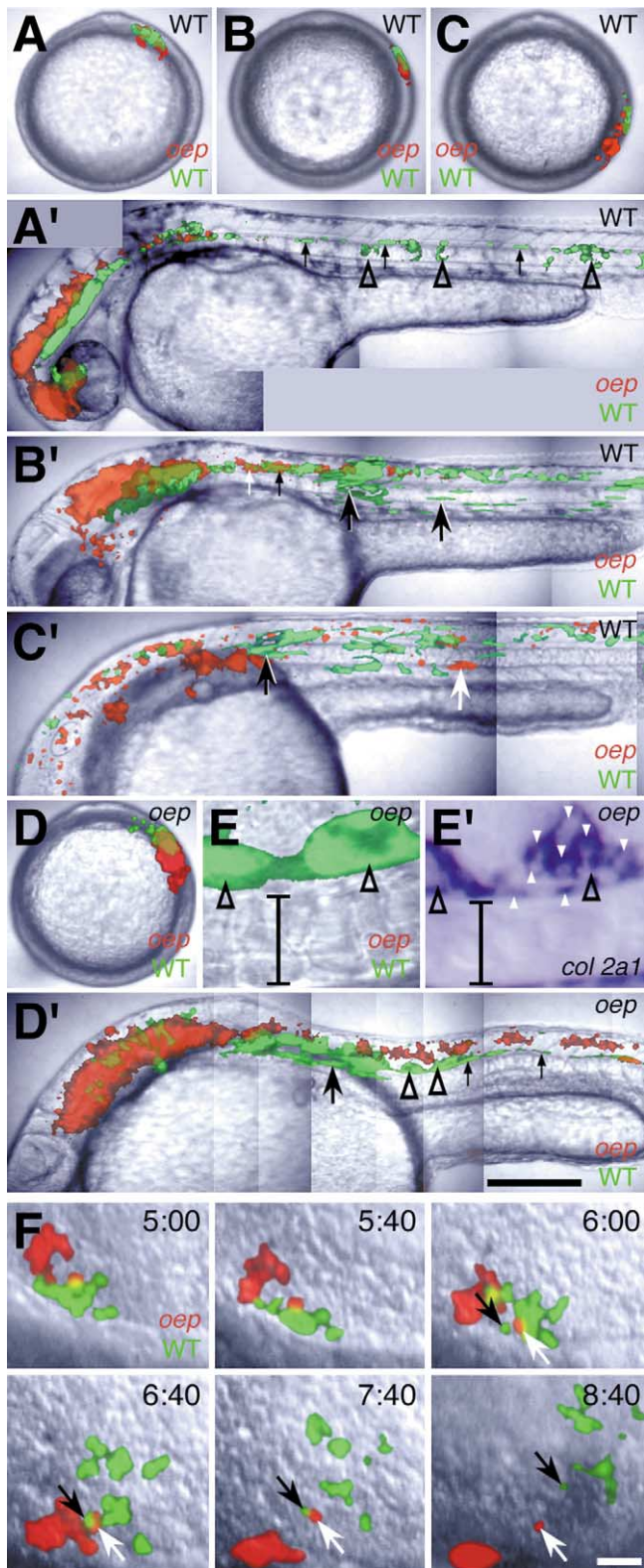
dorsal compaction. This difference between mutant and wild-type was greatest when cells were placed on the lateral side of the embryo and exaggerated further when cells were placed in a mutant host (Fig. 4D). Mutant cells tended to give rise to ectodermal fates compared to mesodermal fates. As above, this difference was increased when mutant and wild-type cells were placed into a mutant host (Fig. 4A′–D′; Table 2). Moreover, wild-type cells placed laterally into a mutant host frequently assumed dorsal fates, such as notochord (Fig. 4D′), and often at ectopic positions (Fig. 4E; *n* = 5 embryos), suggesting that mutant and wild-type cells exhibit differences in their associative properties as well as differences in motility. Although not incorporated into the mutant notochord, this wild-type tissue could induce floorplate gene expression in the mutant neurectoderm (Fig. 4E′), demonstrating that the wild-type notochord had retained its normal inductive capabilities.

Besides biases in cell fate, there were biases in cell position. Mutant derived mesoderm tended to be located posterior of wild-type derived mesoderm (Table 2). This would be expected if mutant cells arrive at the midline later than wild-type cells (Warga and Kimmel, 1990). Thus, mutant donor cells produced less mesendoderm, and that which formed tended to be located posteriorly. It should be noted that, despite the small proportion of mutant donor cells transplanted into a wild-type host, the cells gave rise to

---

ventral spinal cord (small arrows), as well as the notochord (open arrowheads), a mesodermal structure. Donor-mutant cells are located solely in ectodermal structures: dorsal brain. (B) Shield stage, a lateral transplant. (B′) 30 h, donor-wild-type cells are located in ventral brain, spinal cord (small black arrow), as well as the myotomes (large black arrows), a mesodermal structure. Donor-mutant cells are located solely in dorsal brain and spinal cord (small white arrow). (C) Shield stage, a lateral transplant. Note that as the transplants become less dorsal, the separation between donor-wild-type and donor-mutant cells increases. (C′) 30 h, donor-wild-type cells are located in dorsal brain, spinal cord, and the myotomes (black arrow). Donor-mutant cells are similarly located in dorsal brain, spinal cord, and the myotomes (white arrow). Mutant-derived muscle however, is not located as anteriorly as wild-type-derived muscle; the position of both arrows indicates for each donor the most anterior muscle cells. (D, E) Transplantation into a mutant host. (D) Shield stage, a lateral transplant, already there is considerable separation between donor-wild-type and donor-mutant cells. (D′) 30 h, donor-wild-type cells are located in brain, floorplate (small arrows), and the myotomes (large arrow). Furthermore, wild-type cells also gave rise to two ectopically located notochord cells (open arrowheads) above the mutant host notochord. Donor-mutant cells are located in brain and dorsal spinal cord. (E) Higher magnification of wild-type-derived notochord cells (open arrowheads), the underlying host notochord is delineated by bracket. (E′) Same field as (E) following in situ hybridization for *αcollogen2a* mRNA (Yan et al., 1995), which is expressed in floorplate and hypochord, but not notochord cells at this stage. Host-derived floorplate cells (small white arrowheads) overlay the wild-type-derived notochord cells (open arrowheads). (F) Selected frames from a recording of a wild-type chimera. Wild-type cells involute, disperse, and converge toward dorsal (right). White arrow follows one isolated mutant cell, which involutes at about the same time as the last involuting wild-type cell (black arrow). Eventually, this mutant cell lags behind its wild-type cohort. The remaining mutant cells formed a tight aggregate that stalled at the margin. Scale bar: 50 μm (F, G).

Fig. 4. Transplanted *oep* mutant cells are biased to form ectoderm rather than mesoderm and exhibit an autonomous behavior to adhere together and move slowly during gastrulation. (A–C) Transplantation into wild-type hosts. By shield stage, many of the donor-wild-type cells have separated from the donor-mutant cells and moved more dorsal. (A) Shield stage; animal pole view, a dorsolateral transplant. (A′) 30 h, donor-wild-type cells are located in ectodermal structures: ventral brain, and floorplate of the

Table 1

Dorsal and vegetal movement of *oep* mutant cells during dorsal compaction

	Genotype	Dorsal	Lateral	Ventral	Animal
Displacement measurement[a] (μm) $\pm$ S.E.	*oep* mutant	6 ± 0.7^c ($n = 10$)	4 ± 0.6^b ($n = 9$)	4 ± 1.2^b ($n = 9$)	19 ± 3^b ($n = 10$)
	wild-type	8 ± 1.3 ($n = 21$)	20 ± 1.7 ($n = 25$)	18 ± 2.6 ($n = 9$)	46 ± 4.7 ($n = 41$)

[a] The point-to-point distance that a cell traveled dorsovegetally between the sphere to 40% epiboly stage in relation to clonally related extraembryonic surface cells (see Fig. 3).

[b] Significantly differs from wild-type controls at $P < 0.001$ for both Wilcoxon Rank-Sum Test and Student's t-test.

[c] Not significantly different from wild-type control ($P > 0.1$).

fates that were rare in the mutant, namely hatching gland ($n = 1$ embryo) and pharyngeal endoderm ($n = 2$ embryos), both derived from prechordal plate mesendoderm. Thus, *oep* mutant cells have the potential to make most mesendodermal fates, but this potential must be severely compromised in mutant embryos.

To better examine the motility phenotype of *oep* mutant cells, we recorded the behavior of donor cells in chimeric embryos during gastrulation (Fig. 4F). We observed that wild-type donor cells scattered and moved toward the margin, involuted into the hypoblast, and converged dorsally. In contrast, mutant donor cells cohered to each other, forming tight aggregates that did not mix with the surrounding wild-type cells. The mutant cells moved very slowly toward the margin, where they typically stalled and rarely appeared to involute before the end of our recordings. Many of the stalled mutant donor cells eventually differentiated into mesoderm by 24 h; presumably, these cells entered the mesendodermal germ layer after our recordings. Some mutant cells did involute during gastrulation, and, as expected, they continued to move slowly, remaining attached together. Although never moving as quickly as wild-type donor cells, the isolated individual *oep* mutant cell (white arrow in Fig. 4F) moved faster than aggregated *oep* cell clumps, suggesting that cell–cell interactions among groups of mutant cells exaggerated the *oep* mutant phenotype. Consistent with this idea, the difference between wild-type and mutant cells was always greater when cells were placed in *oep* mutant hosts. Thus, *oep* is cell-autonomously required for cell–cell inter-

actions that appear to mediate changes in cell adhesion when cells migrate.

Cell specification in early oep blastulae

What with the involvement of *oep* in the Nodal signaling pathway, alterations in cell morphology and cell movement could be the result of changes in cell specification. Therefore, we assayed the initial state of zygotic *oep* mutants using markers of cell specification for all three germ layers both before and just after the beginning of gastrulation (Fig. 5). Using wild-type siblings to carefully stage zygotic *oep* embryos, we characterized the early distribution of endoderm in the *oep* hypoblast using an antibody to Forkhead Domain 2 (Warga and Nüsslein-Volhard, 1999), also known as FoxA3. Fkd2 is first localized to nuclei of dorsal marginal cells at 30% epiboly and the syncytial nuclei of the yolk cell. At shield stage, Fkd2 is found in the endodermal progenitors on the yolk cell as well as in the axial progenitors of the prechordal plate mesendoderm, floorplate, and notochord (Fig. 5A). Expression of Fkd2 in these cell types as well as in the yolk syncytial layer persists through the remainder of gastrulation and early somitogenesis (Fig. 5B–F). At 30% epiboly, the spatial distribution of Fkd2 appeared normal in *oep* mutant blastulae (data not shown). However, at shield stage, Fkd2-expressing cells in the shield and endodermal domain were located more marginally and were more densely crowded together (Fig. 5A'). By 70% epiboly, the mutant axis was invariably shorter and wider, and the endodermal progenitors more clumped than wild-type (Fig.

Table 2

Fate and position of *oep* mutant donor cells

	Host genotype	Donor genotype	Dorsal[a]	Lateral[a]	Ventral[a]
Percentage of donor-derived cells forming mesoderm[b] $\pm$ S.E.	wild-type	*oep*	18 ± 8^d	36 ± 9^d	92 ± 8
		wild-type	46 ± 11 ($n = 4$)	66 ± 9 ($n = 18$)	93 ± 6 ($n = 11$)
	oep	*oep*	32 ± 18^d	67 ± 33	100 ± 0
		wild-type	75 ± 14 ($n = 7$)	84 ± 16 ($n = 3$)	100 ± 0 ($n = 3$)
Percentage of hosts where wild-type donor-derived mesoderm was more anterior[c]	wild-type	WT & *oep*	93 ($n = 14$)	94 ($n = 17$)	90 ($n = 10$)
	oep	WT & *oep*	100 ($n = 7$)	100 ($n = 3$)	67 ($n = 3$)

[a] Position at shield stage.

[b] The number of cells that formed mesoderm divided by the number of cells that formed mesoderm plus the number of cells that formed ectoderm. n indicates the number of host embryos analyzed.

[c] In some cases, both donors gave rise to mesoderm at the same position (a tie). These animals were excluded from this category.

[d] Significantly different at the $P < 0.001$ level between the wild-type and *oep* mutant results.

5B′–D′). In appearance, these altered patterns mirror what we observe in vivo. After gastrulation, the number of Fkd2-positive endodermal and prechordal cells dropped significantly, but was not eliminated (Fig. 5E′ and F′). Consistent with this observation, pharyngeal endodermal pouches, as revealed by Zn5 staining (Fig. 5U), were fewer in number, but were not completely abrogated. Thus, despite their morphologically abnormal appearance, endodermal precursors are properly specified in *oep* mutants, and a fraction of these cells take their appropriate fate.

In general, the early spatial distribution of many ectodermal and mesendodermal markers in mutant embryos supported these conclusions (Fig. 5G–T), that is, early specification events appear to be normal. When we noted changes in pattern of gene expression, the changes tended to follow the timing of key morphogenetic events. For example, the expression of *goosecoid* in the dorsal organizer region (Schulte-Merker et al., 1994; Thisse et al., 1994) was initially normal (Fig. 5G), but between 30 and 40% epiboly, when dorsal compaction coalesces cells toward the organizer region (Warga and Nüsslein-Volhard, 1998), *goosecoid* expression began to fade (Fig. 5H). The expression of *gata5* in the endoderm and cardiac precursor domain (Reiter et al., 1999; Rodaway et al., 1999) was normal at the onset of involution (Fig. 5I), but absent (data not shown) or less extensive shortly later (Fig. 5J). Striking changes were exhibited by the markers *sox17* (Alexander and Stainier, 1999) and *axial* (Schier et al., 1997), but neither gene is expressed in the endoderm until after the onset of involution. In agreement with previous studies (Alexander and Stainier, 1999; Schier et al., 1997), both reflected diminished numbers of endodermal cells in the mutant gastrula (Fig. 5O–R). The mesodermal markers *snail1* (Hammerschmidt and Nüsslein-Volhard, 1993; Thisse et al., 1993) and No Tail (Schulte-Merker et al., 1992) appeared normal at germ ring stage (Fig. 5K and S), but expression in the mutant gastrula reflected the defects in convergence of cells to the midline (Fig. 5L and T). In summary, changes in pattern of gene expression between wild-type and *oep* mutant embryos appeared to follow observed defects in key morphogenetic events and generally resulted in reduced expression of developmental markers.

Unexpectedly, rather than reflecting a loss of mesodermal specification in the *oep* mutant, *snail1* expression in the hypoblast was expanded. Similar results were observed with the mesodermal markers *spadetail* (Griffin et al., 1998) and *tbx6* (Hug et al., 1997) (data not shown). We also examined the ectodermal marker *mariposa*. Rather than reflecting a gain of ectoderm in the mutant which might be expected in a mutant that might have reduced mesodermal specification, expression in the dorsal neurectoderm (Varga et al., 1999) was reduced at shield stage (Fig. 5M) and later absent, as previously reported (Hammerschmidt et al., 1996), from the dorsoanterior domain (Fig. 5N). These changes, which also occur after morphological changes, may reflect secondary effects due to lack of inductive properties of the hypoblast.

Activin does not rescue defective cell motility in the oep mutant

To test the hypothesis that *oep*-mediated cell motility is dependent on downstream effects of the Nodal signaling pathway, we activated downstream targets of this pathway by misexpressing Activin, which rescues aspects of the *oep* mutant phenotype, such as cyclopia and the reduction in prechordal-derived tissues (Gritsman et al., 1999). If Activin rescues aspects of the *oep* phenotype by restoring normal specification, than motility defects that are due to altered specification should be rescued. We did not find this to be the case.

We injected Activin mRNA into mutant embryos at the 1-cell stage and later injected a single blastomere with fluorescent lineage tracer at the 2000-cell stage. The behavior of the labeled cells was then observed in wild-type and mutant blastulae. The genotypes of these embryos were later confirmed by genotyping (Fig. 6G). In contrast to cells in wild-type blastulae, cells in mutant blastulae exhibited marked cohesiveness, failing to scatter or move dorsovegetally during the period of early epiboly and dorsal cell compaction (Fig. 6A, B and H). When cells in wild-type gastrulae underwent convergent-extension, cells in mutant gastrulae remained tightly aggregated failing to disperse along the animal–vegetal axis and converged much more slowly compared with cells in the wild-type (Fig. 6C and D).

Whereas injections of *activin* failed to rescue defective cell cohesion and cellular rearrangement of *oep* mutant embryos, the injections did successfully rescue aspects of the *oep* mutant phenotype (Fig. 6C′, D′, E and F) similar to that shown in previous reports (Gritsman et al., 1999). Pertinent to this apparent contradiction, we noticed that the prechordal-mesendoderm of *activin*-injected embryos was notably larger during gastrulation (arrow in Fig. 6C and D). In *Xenopus,* application of Activin to explanted cells can induce a range of fates including prechordal mesoderm (Green et al., 1992; McDowell and Gurdon, 1999). Indeed, in the older wild-type and mutant *activin*-injected embryos, we found more prechordal- and chordomesodermal-derived cells than normal (data not shown).

squint;cyclops mutants display motility phenotypes opposite of oep embryos

To test the hypothesis that *oep*-mediated cell motility is dependent on the direct effects of Squint/Cyclops signaling, we examined the behavior of cells in embryos that were double mutant for *cyclops* and *squint*. Like earlier experiments, we labeled single cells at the blastoderm margin in 1000-cell-stage embryos and then recorded them by time-lapse video microscopy. These experiments were numerically challenging because embryos from clutches produced by fish that are heterozygous for both *cyclops* and *squint* yield only 1 double homozygous mutant per 16 embryos. Hence, we recorded embryos in groups of 10–20 individuals with the aid of a computer-controlled stage, and on the average, one double
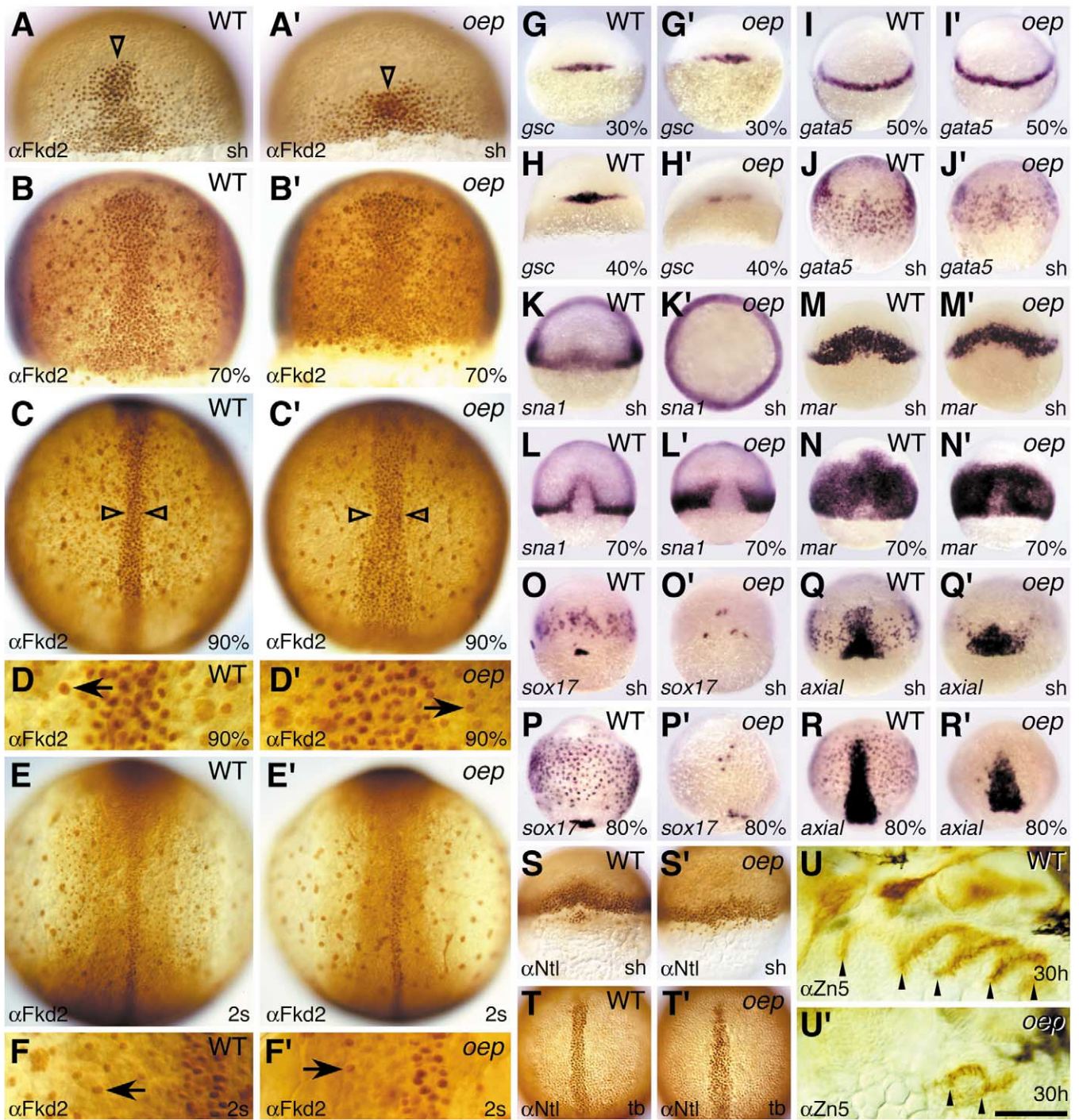
Fig. 5. Early specification in the *oep* mutant is normal. (A–F) Wild-type and mutant siblings visualized with αFkd2 antibody, which labels endoderm (arrows), axial mesendoderm (arrowheads), and yolk syncytial nuclei. (A) Shield stage; dorsal view; arrowhead indicates the leading edge of the dorsal hypoblast. (B) 70% epiboly; dorsal view. (C) 90% epiboly; dorsal view. (D) Higher magnification of (C). (E) Two-somite stage; dorsal view. (F) Higher magnification of (E). (G–R) Wild-type and mutant siblings visualized by whole-mount in situ hybridization. Expression of: (G) *goosecoid;* 30% epiboly, dorsal view. (H) *goosecoid;* 40% epiboly, dorsal view. (I) *gata5;* 50% epiboly, side view. (J) *gata5;* shield stage, dorsal view. (K) *snail1;* germring stage, dorsal view and animal pole view. (L) *snail1;* 70% epiboly, dorsal view. (M) *mariposa;* shield stage, dorsal view. (N) *mariposa;* 70% epiboly, dorsal view. (O) *sox17;* shield stage, dorsal view. (P) *sox17;* 80% epiboly, dorsal view. (Q) *axial,* shield stage, dorsal view; axis darker staining. (R) *axial;* 80% epiboly, dorsal view. (S–U) Wild-type and mutant siblings visualized by whole-mount antibody staining. (S) αNtl; germring stage, dorsal view. (T) αNtl; tailbud stage, dorsal view. (U) αZn5; 30 h, side view, arrowheads indicate pharyngeal pouch endoderm. Scale bar: 30 μm (D, F), and 100 μm (U).

mutant was obtained per experiment which we later confirmed by genotyping (see Materials and methods). We found that cells in *squint;cyclops* mutant blastulae scattered normally dur-

ing radial-intercalation movement and did not cohere whether they were located on the ventral or lateral sides of the embryo; this is a completely wild type phenotype (Fig. 7). Interestingly,
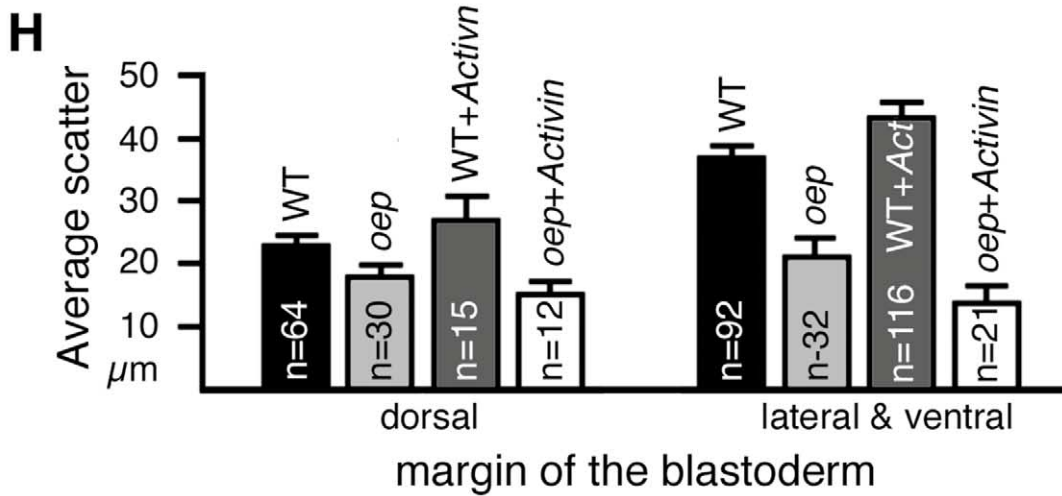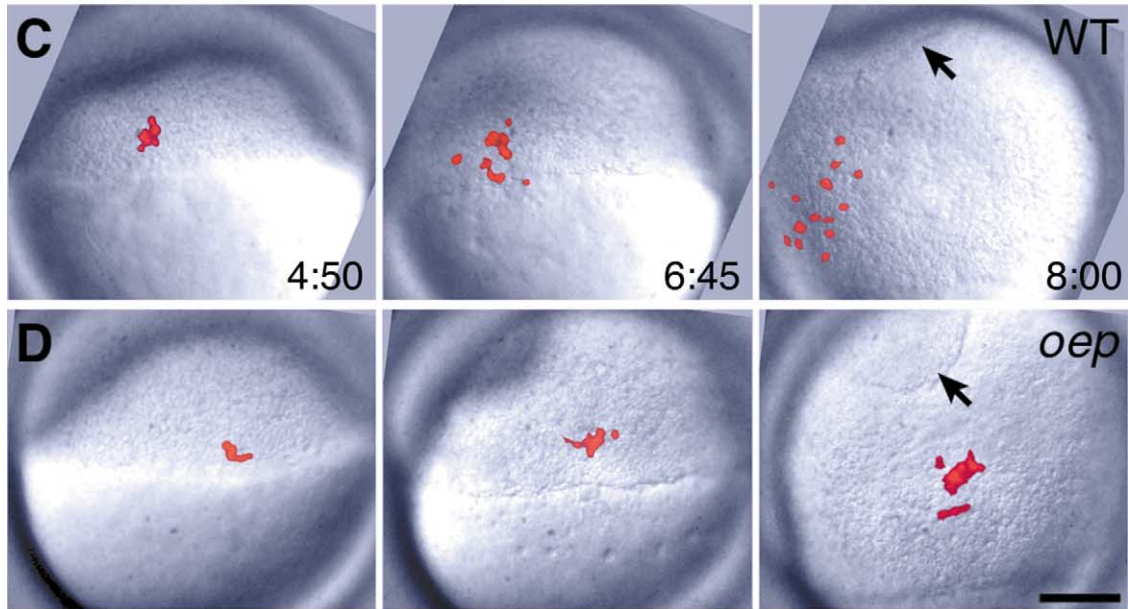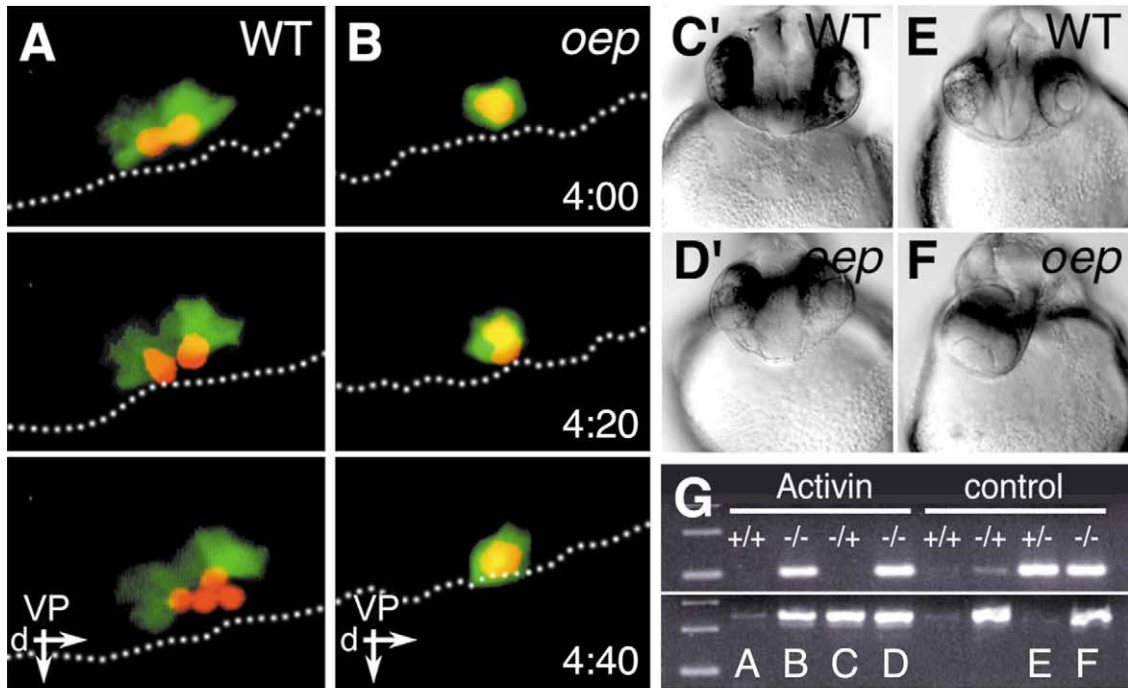
on the dorsal side of the double mutant, where cells normally coalesce due to dorsal compaction, mutant cells displayed an opposite phenotype from that seen in *oep* mutants: cells scattered to twice the degree of cells in wild-type embryos (Fig. 7D). In our time-lapse recordings, we observed a remarkable meandering of dorsal cells in double mutant embryos, with individual cells moving much faster than any such cells in wild-type embryos (Fig. 7A and B). This unusual behavior, which also appeared to correlate with the defect in dorsal compaction, was also observed on the dorsal side of embryos homozygous mutant for *squint* that were heterozygous mutant for *cyclops* ($n = 3$ out of 4 embryos) as well as in 1 homozygous *squint* mutant that was homozygous wild-type for *cyclops,* indicating that this aberrant dorsal behavior may be attributed to loss of Squint activity.

Whereas the hypoblast appears absent in *squint;cyclops* mutants, occasional cells did appear to involute during early gastrulation ($n = 4$ cells in 2 embryos). These cells, which were at or near the margin of the blastoderm at the beginning of our recordings, moved deep, passing beneath other labeled cells towards the animal pole (Fig. 7B). Because these embryos lack a definitive hypoblast layer, it was difficult to judge if this process was entirely normal. Nevertheless, cells of the double mutant that moved under the epiblast behaved as hypoblast cells of wild-type embryos (Fig. 7A). Moreover, *squint;cyclops* mutant cells did not display a tendency to adhere together (compare Fig. 7B and C). Altogether, these results indicate that the nature of the motility defect in *oep* mutants is not a result of the combined lack-of-function of the two Nodal related genes. Indeed, many of the motility aspects of the double mutant phenotype appear the opposite of that observed in the *oep* mutant, especially on the dorsal side of the blastoderm where *squint* is initially expressed (Fig. 8E).

The oep cell motility defect extends to the animal pole

In our initial work, we focused our experiments on the margin of the blastoderm because zygotic transcripts of the zebrafish *nodal*-related genes are restricted to the margin of the blastoderm after the MBT (Erter et al., 1998; Feldman et al., 1998; Rebagliati et al., 1998; Sampath et al., 1998). We confirmed these results, presented above, in carefully staged embryos just before the onset of epiboly and shortly thereafter

(Fig. 8E–H). While the kinetics, synthesis, and diffusion of Squint or Cyclops are unknown, misexpression studies suggest that Squint acts within a distance of six to eight cell diameters and Cyclops within two cell diameters (Chen and Schier, 2001), distances that only extend from the blastoderm marginal region midway to the animal pole. Hence, we examined the behavior of cells at the animal pole, a region that is more than 20 cell diameters from the marginal region and should, in principle, be free from the influence of Nodal-related signals.

In normal blastulae, animal pole clones scatter to a greater extent than clones at the margin because the process of radial intercalation is more extreme at the animal pole (Wilson et al., 1995). Surprisingly, in *oep* mutant blastulae, the cells of animal pole clones exhibited marked cohesiveness (Fig. 8C). As with marginal clones, these differences were highly statistically significant (Fig. 8D) and occurred well before the onset of gastrulation, the time when Nodal-expressing dorsal hypoblast cells only just begin their advance toward the animal pole. Indeed, the slowing of epiboly observed in occasional clutches of *oep* mutants (our unpublished data) may result from perturbation of ordered radial intercalations of cells during blastula stages, because cells deep within the blastoderm (which intercalate radially outwards) also exhibit marked cohesiveness (data not shown). In striking contrast, the behavior of animal pole cells in *squint;cyclops* mutant blastulae were normal and indistinguishable from wild type cells (Fig. 8A, B, and D). In summary, these data show that *oep* function is required for mediating cell–cell interactions in regions of the embryo far from the theoretical source of combined Squint/Cyclops signaling.

Discussion

In the oep mutant, changes in specification in the blastula and gastrula follow changes in cell motility and morphogenesis

Gastrulation movements are abnormal in *oep* mutants. It is hypothesized that perturbations in Nodal-related signaling cause changes in cell fate and that, in turn, these changes result in altered cell movement (Carmany-Rampey and Schier, 2001; Gritsman et al., 1999, 2000). However, at least in the zygotic *oep* mutant, we found that changes in

Fig. 6. Activin rescues the zygotic *oep* phenotype, but not defective cell cohesiveness and migration. (A–D) Examples of lateral clones in four embryos injected with *activin* mRNA at the one-cell stage. (A, B) Wild-type and mutant sibling during doming to 40% epiboly. Each clone initially consists of two deep cells (red) and one to two extraembryonic surface cells (green); dotted line indicates the blastoderm margin. In the mutant, both deep cells divide between 4:00 to 4:40 h, but remain tightly aggregated. Furthermore, the clone does not move toward dorsal and away from its extraembryonic siblings during dorsal cell compaction. (C, D) Wild-type and mutant sibling during 40–80% epiboly. In the mutant, cells cohere even while involuting and generally converge very little compared with the cells of the wild-type sibling. Note that Activin does induce more prechordal plate mesendoderm (arrow) in the wild-type and the mutant. Dorsal is toward left. (C′, D′) Same two embryos at 30 h of development, showing rescue of cyclopia and brain. Both embryos additionally had greater than normal amounts of notochord and hatching gland, a prechordal plate derived structure (data not shown). (E, F) Uninjected wild-type and mutant sibling. (G) Confirmation of genotype by PCR and gel electrophoresis. The first four lanes are experimental embryos (A–D), and the last four lanes are uninjected siblings, including (E, F). Only the mutant alleles amplify a product; see Materials and methods for further details. (H) The median distance between clonal cells at 40% epiboly depending on dorsoventral location. Activin misexpression has no effect on mutant cell cohesiveness or cell scattering during early epiboly. Scale bar: 50 μm (A, B), 200 μm (C′, D′, E, F).

morphogenesis always precede changes in cell specification. Shortly after the MBT, in both wild-type and mutant midblastula embryos, markers of cell specification are overtly normal. Not until the mid-gastrula are there effects on cell motility that can be definitively attributed to failure of Squint and Cyclops activity.

Such results suggest an alternative or additional function for *oep,* one that operates parallel to the Nodal pathway rather than in the Nodal pathway itself. Evidence for this hypothesis is found also in the mouse, where markers such as *Brachyury* and *Fgf8,* although mislocalized, are expressed at *normal* levels in the *cripto* mutant (Ding et al., 1998; Xu et al., 1999), but not expressed at all in the *nodal* mutant (Brennan et al., 2001). Thus, an additional function of *oep* may be to maintain normal contacts among groups of cells. Defective regulation of mesendodermal markers would be consistent with a lack of inductive interactions between cells, interactions that would be perturbed by abnormal adhesion between layers of cells. Altered patterns of gene expression would be only expected after changes in cell adhesiveness, which in turn cause corresponding changes in cell movement, ultimately leading to changes in morphogenesis.

### *oep-mediated motility is independent of Squint and Cyclops signaling*

If *oep* has additional functions that act in pathways parallel to the Nodal pathway, then these functions would be independent of Nodal function. To date, *squint* and *cyclops* are the only two nodal-related genes that have been identified in zebrafish, and both of these genes have essential and overlapping functions in mesendoderm formation (Feldman et al., 1998). We found that many of the aspects of cell motility that are perturbed in *oep* mutants are completely normal in *squint;cyclops* double mutants. Furthermore, at the animal pole, where Squint and Cyclops signaling are absent, *oep*-mediated cell motility is not normal. Lastly, upon misexpressing Activin in *oep* mutants (which *rescues* mesendodermal fate), cell motility is *not* rescued. The simplest interpretation of our results is that *oep* has additional functions for morphogenetic cell behavior and that these functions are independent of Squint and Cyclops signaling, the two Nodal-related genes of zebrafish.

It is possible that some maternal Nodal activity remains in the double mutant, from either undiscovered Nodal-like genes or from maternal contributions of the known genes. Just detectable levels of *squint* transcripts have been seen maternally by in situ hybridization (Gore and Sampath, 2002) and by RT-PCR (Rebagliati et al., 1998), and nothing is known about the abundance and stability of the Squint protein. A narrow interpretation of our experiments is that *oep*-mediated cell motility is independent of zygotic expression of *squint* and *cyclops.* However, our observation that injections of Activin, which compensate for the loss of nodal-related signaling (Thisse et al., 2000), but fail to rescue defective *oep*-mediated cell motility, suggests that our results are general and apply to all Nodal signaling pathways, known and unknown.

Our interpretation contrasts with the interpretations gleaned from studies on the maternal-zygotic *oep* mutant, where Squint and Cyclops signaling does not seem to be operating. In this case, it is reasonable that the effects on cell behavior are likely to be largely the result of lack of mesendodermal specification, for there is almost no mesendodermal specification. Few if any cells involute into the hypoblast and almost all anterior mesendodermal structures are missing. Moreover, markers that specify dorsal structures are absent in the maternal-zygotic mutant during very early epiboly (Gritsman et al., 1999), when motility appears normal in the zygotic mutant. Nevertheless, based on our present work, it seems possible that a larger component of the maternal-zygotic *oep* cell motility phenotype could, in fact, be independent of Squint and Cyclops activity, and studies must be done to determine which functions are dependant on *oep*-mediated cell motility itself in the maternal-zygotic mutant.

Fig. 7. *squint;cyclops* mutant cells do not cohere and show an increased tendency to scatter dorsally. (A–C) Video composite images of dorsal marginal clones between 50 and 80% epiboly from selected frames of the video recording. (A′–C″) A subset of each clone is graphically displayed as a line tracing measured directly from the records of the video recording. (A′–C′) Face view superimposed on same embryo shown in the video composite, tracings orient exactly with the positions of the clone. Color indicates depth. As cells involute, they go from superficial (blue) to deep (red). White circle indicates end of tracing; thick yellow tracings are forerunner cells. (A″–C″) Video composite showing a computer rotated edge view distorted to fit the curvature of the embryo and superimposed on the leftmost side of same embryo (for a size reference only). Color indicates depth; thick tracings are forerunner cells. (A–A″) Labeled wild-type cells involute singly and disperse within the advancing axial hypoblast. Black arrow indicates the first cell to involute; asterisk indicates cells that become forerunner cells; arrowheads indicate the margin. (B–B″) Labeled *squint;cyclops* mutant cells abnormally scatter along the margin (arrowheads). During gastrulation, some cells appear to involute. Black arrow indicates a cell that moves away from the margin beneath other labeled cells; white arrowhead indicates a cell that undergoes aspects of this movement, but never contacts the margin and after passing beneath other cells of the clone returns superficial. The remainder of the cells in this clone appeared to meander randomly around one another as isolated cells: one such cell is indicated with the white arrow. (C′–C″) Labeled *oep* mutant cells adhere together even while involuting and migrating within the dorsal hypoblast. Black arrow indicates the first cell to involute; asterisk indicates cells that become forerunner cells; arrowheads indicate the margin. (D) The median distance between clonal cells at 40% epiboly depending on dorsoventral location. *oep* mutant clones significantly differ from *squint;cyclops* mutant clones and wild-type controls (parenthesis next to wild-type indicate whether they are *oep* or *squint;cyclops* related siblings) at $P < 0.001$ for Wilcoxon Rank Sum Test. In addition, *squint;cyclops* mutant clones significantly differ ($P < 0.001$) from wild-type controls on the dorsal side, indicating that dorsal compaction movement is abnormal in these embryos. Scale bar: 125 μm.
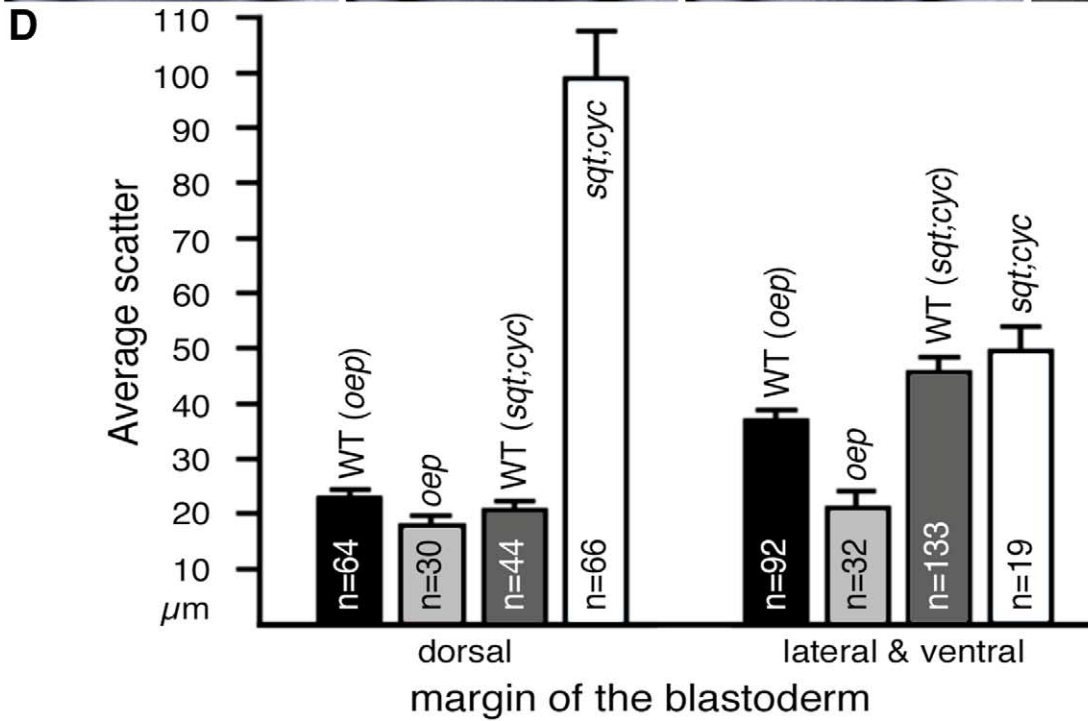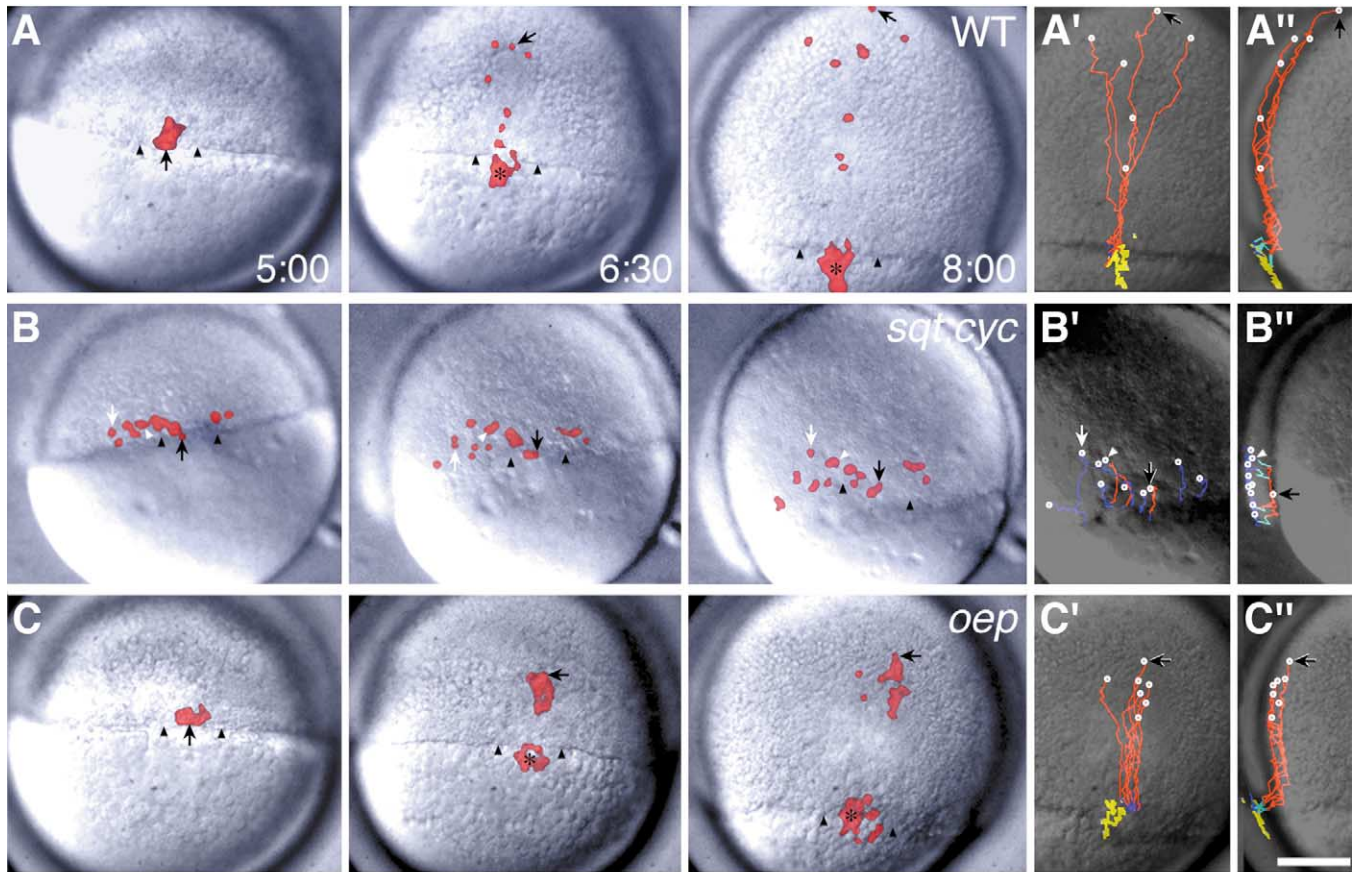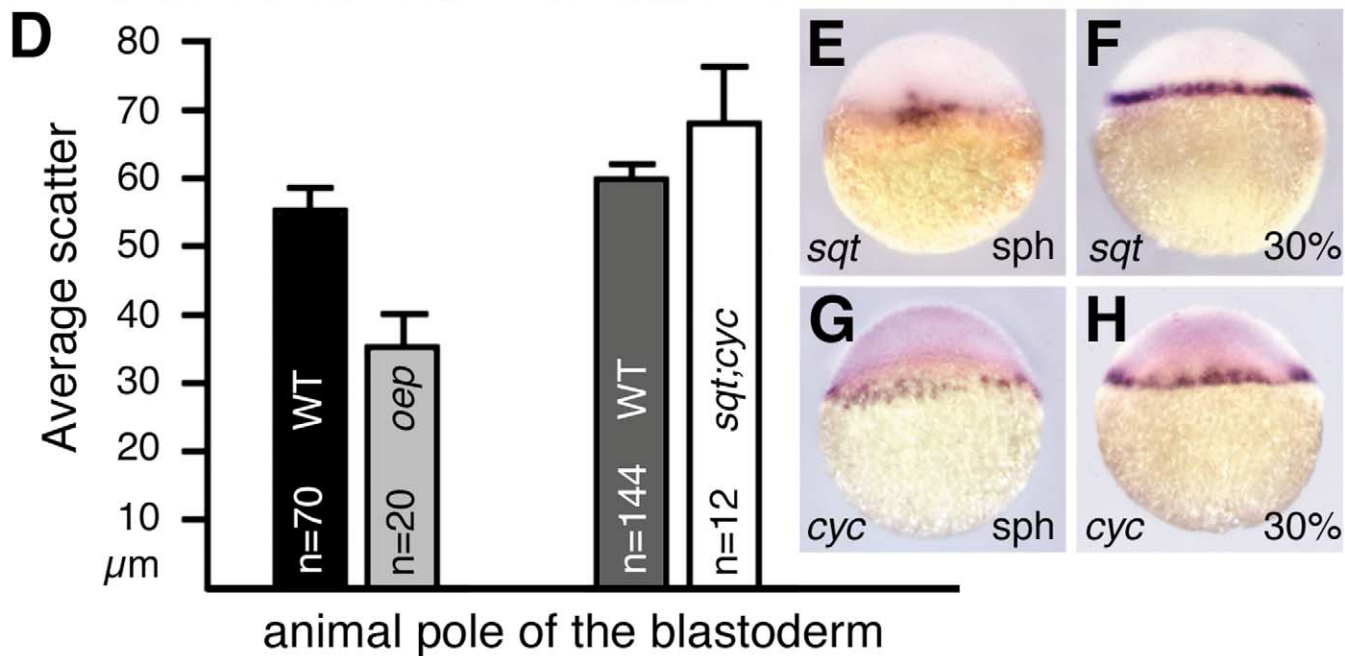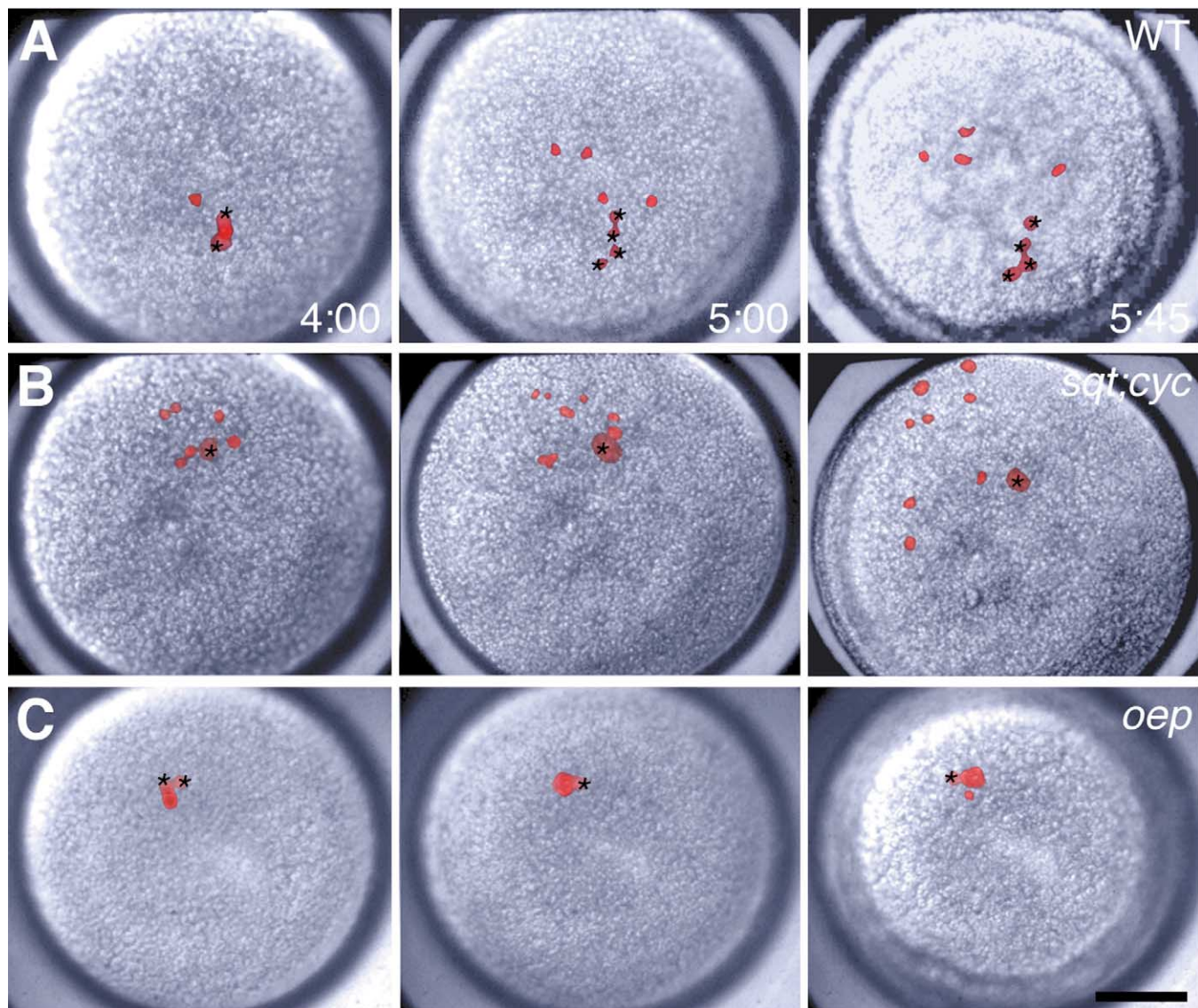
Oep is necessary in a cell-autonomous but indirect manner for proper specification of mesendodermal fate

Using cell transplantation, we have shown that specification of cell fate in *oep* embryos is cell autonomous as assayed both for germ layer and anterior–posterior position. Mutant cells tend to form more ectoderm when compared with wild-type cells, and if mutant cells make mesendoderm, they tend to be located more posterior to wild-type mesendoderm. Our marker studies do not indicate a reduction of mesendodermal territories in mutant embryos, and later it is unclear if the extent of mesodermal tissues is reduced. Indeed, the name "One-Eyed Pinhead" calls attention to the reduction of the head and eyes in the mutant, which are ectodermal tissues.

These changes in fate may be caused by the inability of mutant cells to move normally in competition with wild-type cells. Perhaps *oep* mutant cells that are initially specified toward mesendoderm cannot move into the hypoblast as quickly as wild-type cells, and thus become respecified to an ectodermal fate. This is seen clearly in our transplants, where we observe a tendency for *oep* cells to aggregate together and remain at the blastoderm margin longer than wild-type cells. Some of these mutant cells never involute and accordingly take ectodermal fates. Of those that do involute, they involute later at a stage when the blastoderm margin is more vegetal. Previous studies have shown that cells that involute earliest have a tendency to become endoderm and hatching gland, whereas cells that involute later become mesoderm (Warga and Kimmel, 1990; Warga and Nüsslein-Volhard, 1999). Additionally, the later a cell involutes into the hypoblast the more posterior its fate (Warga and Kimmel, 1990). Thus, our results correlate such changes in cell fate with the time at which donor cells involute into the hypoblast.

In our transplantation experiments, there are changes in the biases to various cell fates but not gaps. In zygotic *oep* mutant embryos, mesendodermal and ectodermal fates both are present; later, tissues such as endoderm and hatching gland are rare, but present. Likewise, in our transplants, we found that many *oep* mutant donor cells become mesoderm, albeit less than in wild-type controls, and rare *oep* cells even become endoderm or hatching gland. These results contrast with those reported by Gritsman et al., (1999) and Schier et al. (1997), who did not find endodermal derivatives. This may be because, in our experiments, we moved only the most marginal cells of the donor to the very margin of the recipient host, done homochronically and shortly after dome

stage. In previous studies, we have found that position and timing are extremely critical in biasing transplant experiments (D.A.K. and R.M.W., unpublished observations).

In the chimeric embryos, donor and host cells that find themselves together in the somite stages often originate from different locations. This occurs because of differences in the speed at which mutant and wild-type cells move. Except for the notochord anlage, the genotypically different cells mix together in the segmentation-stage embryo, and the heterogeneous tissues seem normal at a histological level at 24 h. Thus, for fate specification, the trajectory which cells follow during gastrulation is not nearly as important as the location where cells reside at the end of gastrulation.

The exception to this rule of mixing is the lack of integration of wild-type cells into the mutant host notochord. Curiously, these notochords formed immediately adjacent to the mutant notochord. The wild-type notochord fragments behaved quite normal in that they were able to induce expression of floorplate markers in the overlying neural tube. This seems inconsistent with the results of Strähle et al. (1997), who observed that wild-type notochord cells are incapable of inducing floorplate in *oep* mutants. One difference in our experiment is the ectopic location of the wild-type derived notochord. In the Strähle et al. study, wild-type notochord cells were integrated in among cells of the mutant host notochord, and the wild-type signal from the notochord could be severely inhibited—or diluted—by mutant cells intercalated amongst the wild-type transplant. Such an effect has been seen with wild-type cells transplanted into the *oep* mutant nervous system, where mutant cells suppress floorplate differentiation of adjacent wild-type cells (Shinya et al., 1999). In our experiments, ectopic wild-type notochord, composed of aggregates of genotypically similar cells, might act together to project a strong signal, a signal that must be stronger than that of the mutant host notochord. We note that Shinya et al. (1999) show a nonautonomous effect of mutant *oep* function on wild-type cells; here, our result demonstrates a nonautonomous effect of wild-type *oep* function on mutant cells.

In summary, the reduction in the relative number of transplanted cells taking mesendodermal fate is not likely the simple result of improper cell fate, as may be the case in the *squint;cyclops* double mutant or maternal-zygotic *oep* mutant (Carmany-Rampey and Schier, 2001; Feldman et al., 2000). Cells unable to move to their normal cellular community might be expected to find some difficulty in assuming their normal cell fates, and furthermore, cells making

Fig. 8. Animal pole cells in *oep* mutant blastula cohere abnormally and do not scatter during early epiboly. (A–C) Scatter by radial-intercalation of animal pole cells between sphere and germ ring stage. (A) Labeled wild-type cells at the animal pole scatter vigorously apart; asterisks denote lightly labeled extraembryonic surface cells. One labeled deep cell was initially located between the two extraembryonic surface cells. (B) Labeled *squint;cyclops* cells at the animal pole show similar scattering. (C) Labeled *oep* mutant cells at the animal pole cohere together except while dividing. There are two cells in the first time point, but four by the latter. (D) The median distance between clonal cells at 40% epiboly. *oep* mutant clones significantly differ from wild-type controls and *squint;cyclops* mutants at $P < 0.001$ for Wilcoxon Rank Sum Test. (E–H) Wild-type embryos visualized by whole-mount in situ hybridization. Expression of: (E) *squint,* sphere stage, dorsal view. (F) *squint,* 30% epiboly, side view. (G) *cyclops,* sphere stage, dorsal view. (H) *cyclops,* 30% epiboly, side view.

inappropriate interactions to other cells may not respond to extracellular signals in a normal manner. Thus, the requirement of Oep for Squint/Cyclops function may in part be to facilitate the reception of signals by proper cell–cell contacts, and such a deficiency may further be amplified by a lack of execution of coordinated movement by cells that have been instructed by earlier Nodal signaling at the blastoderm margin.

Avoidance of involution into the zebrafish hypoblast by groups of oep mutant cells: autonomous or nonautonomous?

We observed that transplanted mutant cells "hang" on the lip of the blastoderm, while other cells are involuting around them. This has not been observed before, and it has interesting implications on the mechanisms that cells use to move into the hypoblast. If involution into the hypoblast is based on the movement of a sheet of cells into the deeper regions of the blastoderm, then cells that are not actively participating in this process should be carried along passively by their neighbors. Instead, mutant cells are able to sort themselves from the involution process. In mutant embryos, wild-type cells reach the blastoderm margin, involute, and converge dorsally, while moving all the time through or around a field of mutant cells. These observations suggest that individual cells move into the hypoblast individually, in a type of movement recently defined as "active" involution (Ibrahim and Winklbauer, 2001).

Our observations on the involution of mutant cells into the hypoblast contrast with those reported by Carmany-Rampey and Schier (2001), who reported that individual mutant cells of maternal-zygotic oep were carried into the hypoblast of a wild-type host, where they did not participate in the formation of the hypoblast. However, there are many differences between their experiments and ours. In their experiments, the transplants were derived from maternal-zygotic oep donors, so one might postulate even fewer cells to enter the hypoblast what with the complete inactivation of the Nodal pathway. However, we suggest that the differences between results are more likely because of the timing and size of our transplantation operations. Our transplantations were done earlier than in the Carmany-Rampey and Schier study, usually one cell cycle before involution occurred. It is our experience that transplanted cells require about 30 min to recover from the transplantation operation. Cells that have not recovered may not have time to form normal cellular contacts, and such cells would tend to be carried along with neighboring cells moving in the host embryo. A more significant difference between the experiments is that our transplants involved more cells, and these cells adhered together. Since interactions between oep cells are defective, such interactions would be more conspicuous in large groups of donor cells. Indeed, we noted that single mutant cells moved more normally than groups of cells. A large raft of mutant cells might make contacts, perhaps

inappropriately, with the outer enveloping layer or the enveloping layer–yolk cell junction, surfaces that are stable relative to the involuting cells of the epiblast, thus slowing the sweep of cells into the hypoblast.

In general, our observations blur the distinction for the traditional autonomous–nonautonomous categories for interpretation of results. Mutant cells not actively participating in a process but being carried along passively by their neighbors, and the lack of movement of a group of cells as opposed to single cells, both might be considered nonautonomous results. In contrast, the ability for mutant cells to actively adhere to other mutant cells and the ability of wild-type cells to individually involute around groups of mutant cells (or involute in mutant embryos), both might be considered autonomous results. Such results might be expected if oep was necessary for the interactions that cells must accomplish when they break and reform cell contacts during the process of cell rearrangement.

oep function may have a role in the regulation of cell adhesion

There are several reasons to think that the motility defects of the oep mutant phenotype are the result of a lack of proper adhesion between cells. In teleosts, the yolk cell is thought to be a normal substrate for migrating cells of the hypoblast (Trinkaus and Erickson, 1983), performing a function similar to the blastocoel roof of Xenopus (Winklbauer et al., 1992). Mutant hypoblast cells do not spread onto the yolk cell as do wild-type cells, and when the mutant blastoderm is detached, few cells remain attached to the yolk cell. Hence, mutant cells seem to lack the normal ability to adhere to the yolk cell. Instead, they seem to show a preference to adhere to one another, first seen as a curious ability for cells to adhere to siblings after cleavage divisions in the blastula stage. This could be caused by an attraction via the midbody left after cell division or it could be that daughter cells are simply close to one another immediately after a cell division, a situation attenuated by the slow pace of cell rearrangements in the mutant. The preference of mutant cells to attach to other mutant cells is cell-autonomous, for when mutant cells are transplanted into a wild-type host, a technique that dissociates cells as they are pulled individually into the transplant pipette, the donor cells do not mingle with the surrounding wild-type cells, but tend to form an aggregate. This aggregate seems worse when the mutant cells are in a wild-type embryo than when they are in a mutant host.

Differences between wild-type and oep cell adhesion may be responsible for the interesting defects during the morphogenesis of the ectopic notochord that we have discussed above. In cases where donor wild-type cells were transplanted into the marginal region of mutant hosts and ended up in the notochord field, wild-type cells formed small patches of ectopic notochord alongside the mutant notochord rather than integrating into it. During

segmentation, *oep* transcripts are almost exclusively localized to the notochord (Zhang et al., 1998). It is during segmentation that cells of the notochord anlage extensively intercalate mediolaterally between one another, lengthening and narrowing this tissue, a process thought to be mediated by cell adhesion (Adams et al., 1990). At some time during notochord elongation, the *oep* mutant cells must have separated from the wild-type cells, and afterwards both groups of cells, mutant and wild type, formed independent notochords. It is notable that the location of wild-type notochord was perturbed, not its specification.

Thus, in a manner not unlike Holtfreter's homotypic adhesion experiments, where it was observed that like cells form stronger attachments with one another than with unlike cells (Townes and Holtfreter, 1955), adhesion characteristics between wild-type and mutant cells appear profoundly different. Molecules that mediate adhesion and de-adhesion are fundamental to both cell movement and to epithelial–mesenchymal transitions. We suggest that, in addition to the role of Oep in the reception of Nodal signaling, Oep regulates some aspect of adhesion, and disruption of this function results in defects in processes that require cell adhesion. Considering the location of Oep on the cell surface, it seems reasonable that an important *oep* function may be to maintain the delicate balance of adhesive and nonadhesive forces that are necessary for cells to navigate the embryo. However, what with the role of Oep in Nodal signaling, the severe phenotype of the *oep* maternal-zygotic mutant cannot be explained wholly in exclusive terms of *oep*-mediated motility. The challenge now is to separate the function of *oep* in Nodal signaling from its function in cell motility.

Note added in proofs. Long et al., Dev. 30, 2303–2316 (2003) have shown the discovery of a third Nodal-like gene called *southpaw*. They noted that the mRNA is not present maternally and the zygotic mRNA is present until segmentation.

References

Adams, D.S., Keller, R., Koehl, M.E., 1990. The mechanics of notochord elongation, straightening, stiffening in the embryo *Xenopus laevis*. Development 100, 115–130.

Alexander, J., Stainier, D.Y.R., 1999. A molecular pathway leading to endoderm formation in zebrafish. Curr. Biol. 9, 1147–1157.

Bianco, C., Adkins, H.B., Wechselberger, C., Seno, M., Normanno, N., De Luca, A., Sun, Y., Khan, N., Kenney, N., Ebert, A., Williams, K.P., Sanicola, M., Salomon, D.S., 2002. Cripto-1 activates Nodal- and Alk4-dependent and -independent signaling pathways in mammary epithelial cells. Mol. Cell. Biol. 22, 2586–2597.

Bianco, C., Kannan, S., De Santis, M., Seno, M., Tang, C.K., Martinez-Lacaci, I., Kim, N., Wallace-Jones, B., Lippman, M.E., Ebert, A.D., Wechselberger, C., Salomon, D.S., 1999. Cripto-1 Indirectly stimulates the Tyrosine Phosphorylation of *erb* B-4 through a novel receptor. J. Biol. Chem. 274, 8624–8629.

Brennan, J., Lu, C., Norris, D., Rodriguez, T., Beddington, R., Robertson, E., 2001. Nodal signalling in the epiblast patterns the early mouse embryo. Nature 411.

Carmany-Rampey, A., Schier, A.F., 2001. Single-cell internalization during zebrafish gastrulation. Curr. Biol. 11, 1261–1265.

Chen, Y., Schier, A.F., 2001. The zebrafish Nodal signal Squint functions as a morphogen. Nature 411, 607–610.

Ding, J., Yang, L., Yan, Y.-T., Chen, A., Desai, N., Wynshaw-Boris, A., Shen, M.M., 1998. *Cripto* is required for correct orientation of the anterior–posterior axis in the mouse embryo. Nature 395, 702–707.

Erter, C.E., Solnica-Krezel, L., Wright, C.V., 1998. Zebrafish *nodal-related 2* encodes an early mesendodermal inducer signaling from the extraembryonic yolk syncytial layer. Dev. Biol. 204, 361–372.

Feldman, B., Dougan, S.T., Schier, A.F., Talbot, W.S., 2000. Nodal-related signals establish mesendodermal fate and trunk neural identity in zebrafish. Curr. Biol. 10, 531–534.

Feldman, B., Gate, M.A., Egan, E.S., Dougan, S.T., Rennebeck, G., Sirotkin, H.I., Schier, A.F., Talbot, W.S., 1998. Zebrafish organizer development and germ-layer formation require nodal-related signals. Nature 395, 181–185.

Gore, A.V., Sampath, K., 2002. Localization of transcripts of the zebrafish morphogen Squint is dependent on egg activation and the microtubule skeleton. Mech. Dev. 112, 153–156.

Green, J.B., New, H.J., Smith, J.C., 1992. Responses of embryonic *Xenopus* cells to Activin and FGF are separated by multiple dose thresholds and correspond to distinct axes of the mesoderm. Cell 71, 2595–2609.

Griffin, K.J.P., Amacher, S.L., Kimmel, C.B., Kimelman, D., 1998. Molecular identification of *spadetail*: regulation of zebrafish trunk and tail mesoderm formation by T-box genes. Development 125, 3379–3388.

Gritsman, K., Talbot, W.S., Schier, A.F., 2000. Nodal signaling patterns the organizer. Development 127, 921–932.

Gritsman, K., Zhang, J., Cheng, S., Heckscher, E., Talbot, W.S., Schier, A.F., 1999. The EGF-CFC protein One-eyed pinhead is essential for Nodal signalling. Cell 97, 121–132.

Hagemmann, C., Blank, J.L., 2001. The ups and downs of MEK kinase interactions. Cell. Signal. 13, 863–875.

Hammerschmidt, M., Nüsslein-Volhard, C., 1993. The expression of a zebrafish gene homologous to *Drosophila snail* suggests a conserved function in invertebrate and vertebrate gastrulation. Development 119, 1107–1118.

Hammerschmidt, M., Pelegri, F., Mullins, M.C., Kane, D.A., Brand, M., Eeden, F.J.M.v., Furutani-Seiki, M., Granato, M., Haffter, P., Heisenberg, C.-P., Jiang, Y.-J., Kelsh, R.N., Odenthal, J., Warga, R.M., Nüsslein-Volhard, C., 1996. Mutations affecting morphogenesis during gastrulation and tail formation in the zebrafish, *Danio rerio*. Development 123, 143–151.

Helde, K.A., Wilson, E.T., Cretekos, C.J., Grunwald, D.J., 1994. Contributions of early cells to the fate map of the zebrafish gastrula. Science 265, 517–520.

Ho, R.K., Kane, D.A., 1990. Cell-autonomous action of zebrafish *spt-1* mutation in specific mesodermal precursors. Nature 348, 728–730.

Hug, B., Walter, V., Grunwald, D.J., 1997. *tbx6*, a Brachyury-related gene expressed by ventral mesendodermal precursors in the zebrafish embryo. Dev. Biol. 183, 61–73.

Ibrahim, H., Winklbauer, R., 2001. Mechanisms of mesendoderm internalization in the *Xenopus* gastrula: lessons from the ventral side. Dev. Biol. 240, 108–122.

Kane, D.A., Kimmel, C.B., 1993. The zebrafish midblastula transition. Development 119, 447–456.

Kane, D.A., Maischein, H.-M., Brand, M., Eeden, F.J.M. v., Furutani-Seiki, M., Granato, M., Haffter, P., Hammerschmidt, M., Heisenberg, C.-P., Jiang, Y.-J., Kelsh, R.N., Mullins, M.C., Odenthal, J., Warga, R.M., Nüsslein-Volhard, C., 1996. The zebrafish epiboly mutants. Development 123, 47–55.

Kannan, S., De Santis, M., Lohmeyer, M., D.J., R.I. Smith, G.H., Hynes, N., Seno, M., Brandt, R., Bianco, C., Persico, G., Kenney, N., Normanno, N., Martinez-Lacaci, I., Ciadiello, F., Stern, D.F., Gullick, W.J., Salomon, C.S. (1997). Cripto enhances the tyrosine phosphylation of Shc and activates mitogene-activated protein kinase (MAPK) in mammary epithelial cells. J. Biol. Chem. 272, 3330–3335.

Kassis, J., Lauffenburger, D.A., Turner, T., Wells, A., 2001. Tumor invasion as dysregulated cell motility. Semin. Cancer Biol. 11, 105–117.

Massagué, J., 1998. TGF-β signal transduction. Annu. Rev. Biochem. 67, 753–791.

McDowell, N., Gurdon, J.B., 1999. Activin as a morphogen in *Xenopus* mesoderm induction. Semin. Cell Dev. Biol. 10, 311–317.

Minchiotti, G., Paisi, S., Liguori, G., Signore, M., Lania, G., Adamson, E.D., Lago, C.T., Persico, M.G., 2000. Membrane-anchorage of Cripto protein by glycosylphosphatidylinositol and its distribution during early mouse development. Mech. Dev. 90, 133–142.

Rebagliati, M.R., Toyama, R., Fricke, C., Haffter, P., Dawid, I.B., 1998. Zebrafish *nodal-related* genes are implicated in axial patterning and establishing left–right asymmetry. Dev. Biol. 199, 261–272.

Reissmann, E., Jornvall, H., Blokzijl, A., Andersson, O., Chang, C., Minchiotti, G., Persico, M.G., Ibanez, C.F., Brivanlou, A.H., 2001. The orphan receptor ALK7 and the activin receptor ALK4 mediate signaling by Nodal proteins during vertebrate development. Genes Dev. 15, 2010–2022.

Reiter, J.F., Alexander, J., Rodaway, A., Yelon, D., Patient, R., Hoder, N., Stainier, D.Y.R., 1999. Gata5 is required for the development of the heart and endoderm in zebrafish. Genes Dev. 13, 2983–2995.

Rodaway, A., Takeda, H., Koshido, S., Broadbent, J., Price, B., Smith, J.C., Patient, R., Holder, N., 1999. Induction of the mesendoderm in the zebrafish germ ring by yolk-derived TGF-β family signals and discrimination of mesoderm and endoderm by FGF. Development 126, 3067–3078.

Salomon, D.S., Bianco, C., De Santis, M., 1999. Cripto: a novel epidermal growth factor (EGF)-related peptide in mammary gland development and neoplasia. Bioessays 21, 61–70.

Salomon, D.S., Bianco, C., Ebert, A.D., Khan, N.I., De Santis, M., Normanno, N., Wechselberger, C., Seno, M., Williams, K., Sanicola, M., Foley, S., Gullixk, W.J., Persico, G., 2000. The EGF-CFC family: novel epidermal growth factor-related proteins in development and cancer. Endocrine-Related Cancer 7, 199–226.

Sampath, K., Rubinstein, A.L., Cheng, A.H.S., Liang, J.O., Fekany, K., Solnicakrezel, L., Korzh, V., Halpern, M.E., Wright, C.V.E., 1998. Induction of the zebrafish ventral brain and floorplate requires *cyclops/nodal* signalling. Nature 395, 185–189.

Schier, A.F., Neuhauss, S.C.F., Harvey, M., Malicki, J., Solnica-Krezel, L., Stainier, D.Y.R., Zwartkruis, F., Abdelilah, S., Stemple, D.L., Rangini, Z., Yang, H., Driever, W., 1996. Mutations affecting the development of the embryonic zebrafish brain. Development 123, 165–178.

Schier, A.F., Neuhauss, S.C.F., Helde, K.A., Talbot, W.S., Driever, W., 1997. The *one-eyed pinhead* gene functions in mesoderm and endoderm formation in zebrafish and interacts with *no tail*. Development 124, 327–342.

Schier, A.F., Shen, M.M., 2000. Nodal signalling in vertebrate development. Nature 403, 385–389.

Schmitz, B., Campos-Ortega, J.A., 1994. Dorso-ventral polarity of the zebrafish embryo is distinguishable prior to the onset of gastrulation. Wilhelm Roux's Arch. Dev. Biol. 203, 374–380.

Schulte-Merker, S., Hammerschmidt, M., Beuchle, D., Cho, K.W., De-Robertis, E.M., Nüsslein-Volhard, C., 1994. Expression of the zebrafish *goosecoid* and *no tail* gene products in wild-type and mutant *no tail* embryos. Development 120, 843–852.

Schulte-Merker, S., Ho, R.K., Herrmann, B.G., Nusslein-Volhard, C., 1992. The protein product of the zebrafish homologue of the mouse T gene is expressed in nuclei of the germ ring and the notochord of the early embryo. Development 116, 1021–1032.

Shen, M.M., Wang, H., Leder, P., 1997. A differential display strategy identifies *Cryptic,* a novel EGF-related gene expressed in the axial and lateral mesoderm during mouse gastrulation. Development 124, 429–442.

Shinya, M., Furutani-Seiki, M., Kuroiwa, A., Takeda, H., 1999. Mosaic analysis with *oep* mutant reveals a repressive interaction between floor-plate and non-floor-plate mutant cells in the zebrafish neural tube. Dev. Growth Differ. 41, 135–142.

Sokol, S., Christian, J.L., Moon, R.T., Melton, D.A., 1991. Injected *Wnt* RNA induces a complete body axis in *Xenopus* embryos. Cell 67, 741–752.

Solnica-Krezel, L., Stemple, D.L., Mountcastle-Shah, E., Rangini, Z., Neuhauss, S.C.F., Malicki, J., Schier, A.F., Stainier, D.Y.R., Zwartkruis, R., Abdelilah, S., Driever, W., 1996. Mutations affecting cell fates and cellular rearrangements during gastrulation in the zebrafish. Development 123, 67–80.

Strähle, U., Jesuthasan, S., Blader, P., Pilar, G.-V., Hatta, K., Ingham, P.W., 1997. *one-eyed pinhead* is required for development of the ventral midline of the zebrafish (*Danio rerio*) neural tube. Genes Funct. 1, 131–148.

Tam, P.P.L., Gad, J.M., Kinder, S.J., Tsang, T.E., Behringer, R.R., 2001. Morphogenetic tissue movement and the establishment of body plan during development from blastocyst to gastrula in the mouse. BioEssays 23, 508–517.

Thisse, B., Wright, C.V.E., Thisse, C., 2000. Activin- and Nodal-related factors control antero-posterior patterning of the zebrafish embryo. Nature 403, 425–428.

Thisse, C., Thisse, B., Halpern, M.E., Postlethwait, J.H., 1994. *Goosecoid* expression in neurectoderm and mesendoderm is disrupted in zebrafish *cyclops* gastrulas. Dev. Biol. 164, 420–429.

Thisse, C., Thisse, B., Schilling, T.F., Postlethwait, J.H., 1993. Structure of the zebrafish *snail1* gene and its expression in wild-type, *spadetail* and *no tail* mutant embryos. Development 119, 1203–1215.

Townes, P., Holtfreter, J., 1955. Directed movements and selected adhesions of embryonic amphibian cells. J. Exp. Zool. 128, 53–120.

Trinkaus, J.P., Erickson, C.A., 1983. Protrusive activity, mode and rate of locomotion, and pattern of adhesion of *Fundulus* deep cells during gastrulation. J. Exp. Zool. 228, 41–70.

Varga, Z.M., Wegner, J., Westerfield, M., 1999. Anterior movement of ventral diencephalic precursors separates the primordial eye field in the neural plate and requires *cyclops*. Development 126, 5533–5546.

Warga, R.M., Kimmel, C.B., 1990. Cell movements during epiboly and gastrulation in zebrafish. Development 108, 569–580.

Warga, R.M., Nüsslein-Volhard, C., 1998. *spadetail*-dependent cell compaction of the dorsal zebrafish blastula. Dev. Biol. 203, 116–121.

Warga, R.M., Nüsslein-Volhard, C., 1999. Origin and development of the zebrafish endoderm. Development 126, 827–838.

Weschselberger, C., Ebert, A.D., Bianco, C., Khan, N.I., Sun, Y., Wallace-Jones, B., Montesano, R., Salomon, D.S., 2001. Cripto-1 enhances migration and branching morphogenesis of mouse mammary epithelial cells. Exp. Cell Res. 266, 95–105.

Westerfield, M., 1993. The Zebrafish Book. University of Oregon Press, Eugene, OR.

Whitman, M., 2001. Nodal signaling in early vertebrate embryos. Themes and variations. Dev. Cell 1, 605–617.

Wilson, E.T., Cretekos, C.J., Helde, K.A., 1995. Cell mixing during early epiboly in the zebrafish embryo. Dev. Gene. 17, 6–15.

Winklbauer, R., Selchow, A., Nagel, M., Angres, B., 1992. Cell interaction and its role in mesoderm cell migration during Xenopus gastrulation. Dev. Dyn. 195, 290–302.

Xu, C., Liguori, G., Graziella Persico, M., Adamson, E.D., 1999. Abrogation of the *Cripto* gene in mouse leads to failure of postgastrulation morphogenesis and lack of differentiation of cardiomyocytes. Development 126, 483–494.

Yan, Y.-L., Hatta, K., Postethwait, J.H., 1995. Expression of a type II collogen gene in the embryonic axis of wild type, *cyclops,* and *no tail* zebrafish embryos. Dev. Dyn. 3, 311.

Yan, Y.-T., Liu, J.-J., Luo, Y., Chaosu, E., Haltiwanger, R.S., Abate-Shan, C., Shen, M.M., 2002. Dual roles of Cripto as a ligand and coreceptor in the Nodal signaling pathway. Mol. Cell. Biol. 22, 4439–4449.

Yeo, C.-Y., Whitman, M., 2001. Nodal signals to Smads through Cripto-dependent and Cripto-independent mechanisms. Cell 7, 949–957.

Zhang, J., Talbot, W.S., Schier, A.F., 1998. Positional cloning identifies zebrafish *one-eyed pinhead* as a permissive EGF-related ligand required during gastrulation. Cell 92, 241–251.